Hepatic Immune Landscape Shifts After Bariatric Surgery

A Potential Mechanism for Liver Repair

ADRIANA CALVO RECASENS

Bachelor's Degree Final Project

Biochemistry and Molecular Biology

Academic Tutor: Antonio Jesús Cortés Espinar

Research Project Directors: Prof. Jorge Joven and Alina Iuliana Onoiu

Tarragona, June 2025

This work was conducted based on results from the Curricular Practices in the Biomedical Research Unit, under the supervision of Prof. Jorge Joven Maried and Alina Iuliana Onoiu.

ABSTRACT

Background and aims: The global prevalence of obesity and MASLD has significantly increased in recent decades. Its severe form, MASH, is associated with higher risks of liver complications and premature death. Bariatric surgery is the most effective long-term treatment for severe obesity, improving MASLD and MASH. Emerging evidence emphasizes the important role of hepatic immune cells in the development of MASH. This study aims to evaluate how bariatric surgery-induced weight loss affects hepatic immune cell populations and their relationship with histological and clinical improvements in MASH.

Methods: We analyzed liver biopsies from 44 patients with severe obesity undergoing two-stage bariatric surgery at Hospital Universitari Sant Joan de Reus. Biopsies were stained with H&E and Masson's trichrome, and patients were classified as non-MASH, uncertain, or MASH. IHC for cell markers such as CD15, CD68, CD56, CD4, CD8, and Galectin-3 was performed. We quantified immune cell populations using QuPath, an AI-based digital pathology tool, while clinical data were extracted from the patients' medical records. Non-parametrical statistical analyses were performed.

Results: Digital pathology revealed a significant increase in $CD15^+$ cells following surgery. Although the overall proportions of $CD68^+$ and $CD4^+$ cells did not change significantly, patients with grater histological improvement had a notable decrease in $CD68^+$ cells and an increase in $CD4^+$ cells. Additionally, the proportion and density of Galectin-3^+ cells tended to decrease in patients who experienced greater improvement in NAS and ballooning. No associations were observed between changes in CD15+ cells and baseline comorbidities.

Conclusion: Our findings show that bariatric surgery not only aids in metabolic recovery and weight loss, but also induces significant immunological changes in the liver. These changes may play a role in resolving MASH by shifting immune environment and cell profiles from pro-inflammatory to anti-inflammatory phenotypes. Our use of digital pathology provided a reliable and objective method for quantifying immune cells, establishing a foundation for future research.

Keywords: Digital Pathology, Immune Cell Profiling, Immunohistochemistry, Liver Inflammation, MASH resolution.

INDEX

ABBREVIATIONS

AI: Artificial Intelligence

APCs: Antigen-Presenting Cells

BMI: Body Mass Index

CD8 T_{RM}: CD8 tissue-Resident Memory T cells

CVD: Cardiovascular Disease

DC: Dendritic Cells

DP: Digital Pathology

FDA: Food and Drug Administration

H&E: Hematoxylin and Eosin

HSC: Hepatic Stellate Cells

HTA: Hypertension

IHC: Immunohistochemistry

IQRs: Interquartile Ranges

KC: Kupffer Cells

MASH: Metabolic-dysfunction Associated Steatohepatitis

MASLD: Metabolic-dysfunction Associated Steatotic Liver Disease

MMPs: matrix metalloproteinases

NAFLD: Non-Alcoholic Fatty Liver Disease

NAS: NAFLD Activity Score

NK: Natural Killer

NKT: Natural Killer T

ROS: Reactive Oxygen Species

SLD: Steatotic Liver Disease

TAG: Triglyceride

T2DM: Type 2 Diabetes Mellitus

Treg: Regulatory T

WHO: World Health Organisation

1. INTRODUCTION

1.1.OBESITY

Obesity is a chronic and complex disease defined by The World Health Organisation (WHO) as abnormal or excessive fat accumulation that presents a risk to health. Its development is shaped by a combination of physiological and genetic predispositions, along with an imbalance between energy intake and expenditure. Over the past five decades, obesity has reached pandemic proportions globally and has become one of the major public health challenges. In 2022, 60% of Europeans were either overweight or obese, highlighting the seriousness of the obesity crisis [1,2].

Globally, obesity is more common in women and tends to rise with age, reaching its peak between the ages of 50 and 65 [2,3]. The disease prevalence has increased significantly across all age groups, rising from 30.4% in 1999-2000 to 42.1% in 2017-2020 (*Figure 1*) *[4].*

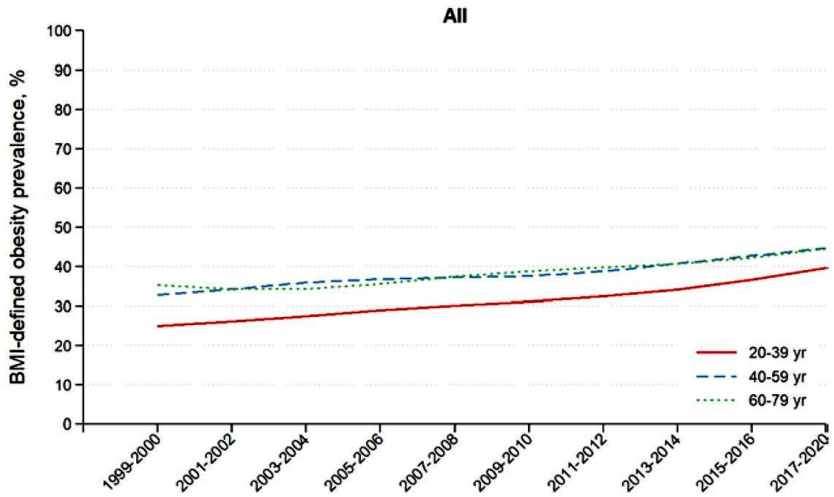

Figure 1. *Temporal trends in age-adjusted obesity prevalence among United States adults, based on BMI, from 1999–2000 to March 2020, stratified by age group [4].*

The most widely used classification for this progressive disease is based on Body Mass Index (BMI), which is determined by dividing a person's weight in kilograms by the square of their height in meters (kg / m^2). Based on this index, individuals are categorized as follows: underweight if their BMI is below 18.5 kg/m2, normal weight if it ranges between 18.5 and

24.9 kg/m2, overweight if it ranges between 25-29.9 kg/m2 and obese if it is 30 kg/m2 or higher (*Figure 2*). Furthermore, obesity is divided into five severity levels: class I (BMI 30-34.9 kg/m2), class II (BMI 35-39.9 kg/m2), class III (40-50 kg/m2), class IV or super obesity (50-59,9 kg/m2), and class V or extreme obesity (60 kg/m2 or higher) [5]. Although BMI is a commonly used metric, it has some limitations: it does not differentiate between muscle mass and fat distribution. To accurately assess health risks, the waist-to-hip ratio is often used as a complementary measure. This ratio reflects abdominal fat accumulation, which is closely linked to metabolic and cardiovascular risks [6–8].

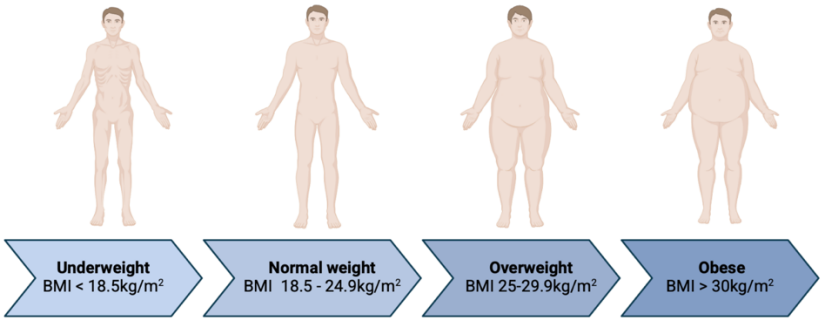

Figure 2. *Body weight classification based on BMI. Image created with BioRender.com.*

Patients with severe obesity experience a lower quality of life and face increased surgical risks, including higher mortality rates. The condition is also closely associated with various comorbidities, such as type 2 diabetes mellitus (T2DM), hypertension (HTA), cardiovascular disease (CVD) and dyslipidemia [9,10]. Lifestyle changes alone are not effective in achieving significant and sustained weight loss or in addressing these related health conditions [11]. As a result, more effective medical interventions are required.

Given these challenges, bariatric surgery remains the most effective and widely used treatment. Among the various types, gastric bypass and sleeve gastrectomy are the most common, with sleeve gastrectomy recognized as the gold standard [12,13]. This procedure removes 80% of the stomach, reducing its capacity and triggering hormonal changes that enhance weight loss [10]. While most patients achieve lasting results, the demand for redo bariatric procedures has increased due to weight regain, insufficient weight loss, and obesity-related comorbidities [14,15].

Moreover, individuals with severe obesity are also at greater risk of developing metabolic dysfunction-associated steatotic liver disease (MASLD) and its progressive form, metabolic dysfunction-associated steatohepatitis (MASH) [16].

1.2.MASLD AND MASH

Steatotic liver disease (SLD) is defined by its hallmark feature: hepatic steatosis, and its etiologies can be grouped based on their association with alcohol intake. Non-alcohol-related SLD primarily refers to MASLD, a condition driven by metabolic dysfunction [17].

MASLD is a complex and multifactorial disorder that occurs alongside at least one cardiometabolic risk factor and is considered the hepatic manifestation of metabolic syndrome. It begins with excessive triglyceride (TAG) accumulation in the liver, leading to steatosis. This accumulation results from an increased influx of fatty acids, derived from circulating lipids influenced by a high-fat diet, enhanced lipolysis in adipose tissue, and *de novo* lipogenesis in the liver [18,19].

As obesity rates rise, MASLD has become increasingly common. Its incidence is estimated at 28-52 cases per 1,000 individuals annually [20]. It is particularly prevalent in severe obese patients, with estimates suggesting that 66-99% of obese patients may develop this condition [12]. Genetic susceptibility plays a crucial role, making certain ethnic groups more prone to this disorder and its complications, further contributing to its increasing impact [21].

Diagnosing MASLD requires the presence of hepatic steatosis affecting at least 5% of the liver tissue, confirmed through imaging or histological examination, while ruling out secondary causes such as alcohol consumption, prolonged use of steatogenic medication, or monogenic genetic disorders [17,20]. Despite its early-stage presentation, MASLD is not a static disease. Without proper intervention, it can progress, with 10-20% of patients developing MASH if not managed correctly [18]. This advanced form is characterized by hepatocellular ballooning, inflammation, and fibrosis, and may evolve into more severe conditions such as cirrhosis and, ultimately, hepatocellular carcinoma (*Figure* 3) [20,22].

However, hepatic steatosis alone is insufficient to promote the progression of MASLD to MASH. Additional cellular stresses, such as lipotoxicity, oxidative stress, and chronic inflammation, play a crucial role in disease development [23].

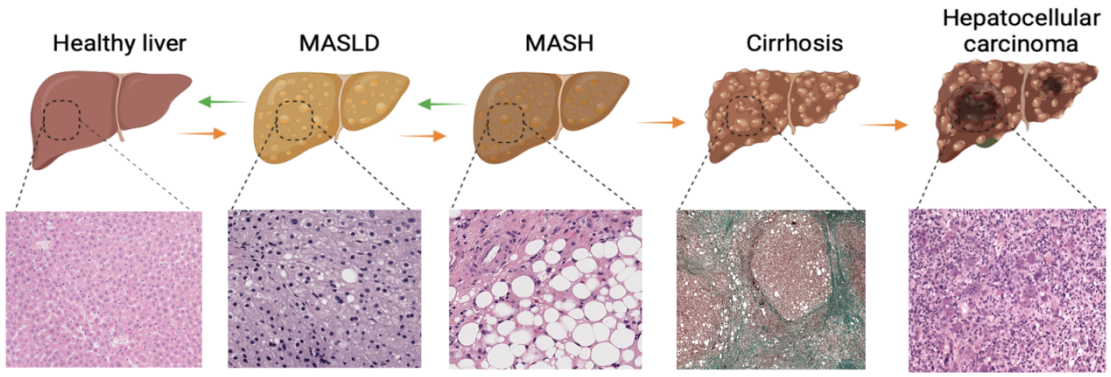

Figure 3. MASLD spectrum. *Schematic representation of MASLD progression. Histological samples are stained with hematoxylin and eosin (H&E) and viewed at 20X magnification, except for the cirrhosis panel, which is stained with Masson's trichrome and viewed at 4X magnification. Orange arrows represent disease progression, while green arrows indicate the potential for reversal [24,25]. Image created with BioRender.com.*

Globally, MASH affects an estimated 1.5–6.45% of the population, with higher prevalence in older men, postmenopausal women, and individuals with multiple metabolic risk factors [26]. These patients are also at higher risk of progressive fibrosis, cirrhosis, and related complications [17].

Although several non-invasive methods -such as blood biomarkers- are available, liver biopsy remains the gold standard for distinguishing MASLD and MASH. To diagnose MASH, *Kleiner et al.* developed the NAFLD Activity Score (NAS), which evaluates steatosis (scored 0-3), hepatocellular ballooning (scored 0-2), and lobular inflammation (scored 0-3). The total NAS ranges from 0 to 8, with a score of 5 or higher supporting a diagnosis of MASH, 3-4 considered uncertain, and a score below 3 indicating non-MASH [27].
However, liver biopsy presents several limitations. It requires evaluation by a trained pathologist and is subject to variability between different observers, as well as inconsistencies in repeated assessments by the same observer over time. In addition, the NAS has limited resolution, which may reduce the accuracy and reliability of the diagnosis [20].

In recent years, bariatric surgery has emerged as a transformative intervention for patients with MASH. This intervention enhances hepatic insulin sensitivity, reduces oxidative stress, and improves lipid metabolism. According to FDA guidance, the resolution of MASH requires the disappearance of features associated with steatohepatitis. This resolution is typically recognized in three different scenarios: (1) MASH resolution without any worsening of fibrosis, (2) an improvement in fibrosis by at least one stage without any worsening of MASH, and (3) a combined outcome in which both MASH resolution and fibrosis improvement occur simultaneously [28]. Patients who achieve greater weight loss are more likely to experience fibrosis improvement, while those who fail to resolve MASH are typically those who do not maintain long-term weight reduction after surgery [13].

Importantly, the progression from MASLD to MASH involves more than just metabolic stress – it is also shaped by immune-mediated inflammation. The inflammatory environment in MASH is primarily controlled by immune system cells. As the disease evolves, the hepatic immune cell landscape changes, contributing directly to the severity of MASH [18]. These immune shifts are crucial in understanding the underlying mechanisms and progression of the disease.

1.3.HEPATIC IMMUNE SYSTEM

1.3.1.THE IMMUNE SYSTEM: INNATE AND ADAPTIVE IMMUNITY

The immune system is a complex network composed of two main components: innate immunity and adaptive immunity, which work together to protect the body from pathogens and maintain homeostasis.

The innate immune system serves as the first line of defense, providing immediate and nonspecific responses through mechanisms such as inflammation and phagocytosis. It relies on physical barriers, such as the skin and mucosal surfaces, and various immune cells that initiate inflammatory responses.

On the other hand, the adaptive immune system generates specific and long-lasting responses by recognizing particular antigens. A key feature of adaptive immunity is its

ability to develop immune memory, which ensures a faster and more effective response if the same pathogen is reencountered.

The interaction between both types of immunity is essential, as the innate mechanisms often help activate the adaptive responses [29–31].

1.3.2.LIVER IMMUNE LANDSCAPE AT HOMEOSTASIS

The liver is a crucial immunological organ that processes approximately 1.5 liters of blood per minute, a volume that needs specialized mechanisms for immune tolerance. These mechanisms prevent unnecessary immune activation while still enabling quick responses to genuine threats, a dual function vital for maintaining balance within the body. The organ's unique environment, populated by various immune cells (*Figure 4*), supports immune regulation. Its extensive vascularization and slow blood flow facilitate direct interactions between circulating immune components and liver resident cells, thereby enhancing exposure to blood and gut-derived antigens [32].

Structurally, the liver is organized into lobules, which are repeating hexagonal units. Within each lobule, hepatocytes are radially arranged around a central vein and connected to the hepatic artery and portal vein via a network of sinusoids. This specialized, fenestrated vascular system is essential for facilitating efficient exchange between blood and hepatocytes and plays a crucial role in maintaining immune homeostasis within the liver microenvironment [33].

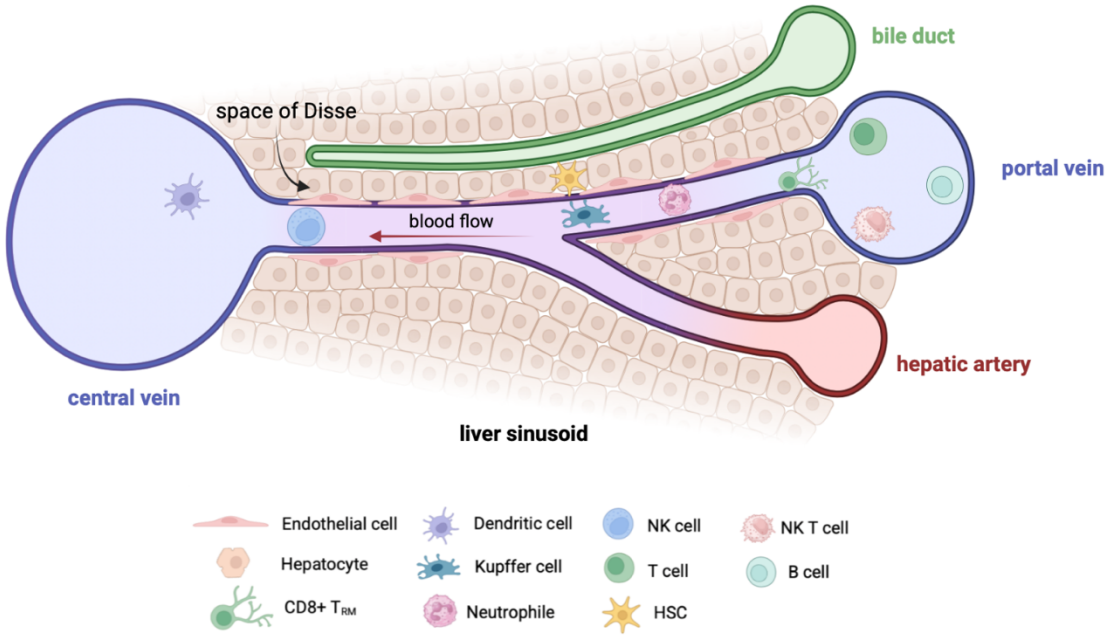

Figure 4. Distribution of key immune cells in the hepatic microenvironment under homeostasis conditions. *Within the hepatic sinusoids, various immune cells are present, including Kupffer cells (KC), CD8-positive and CD4-positive T cells, natural killer (NK) cells, monocytes, natural killer T (NKT) cells, CD8 tissue-resident memory T cells (CD8 TRM), dendritic cells (DC), and B cells. The liver lobules exhibit a polarized immune system known as immune zonation, where myeloid and lymphoid resident immune cells, such as KC, neutrophils, NK cells and B cells, are predominantly found in periportal regions. Additionally, KC can interact with hepatic stellate cells (HSC) located in the space of Disse [33]. Image created with BioRender.com.*

A key component of hepatic immunity is the reticuloendothelial system, primarily consisting of KC and DC. KC are the main resident macrophages in the liver; they originate during embryonic development and are maintained in a healthy adult liver through self-renewal. These cells efficiently engulf pathogens, eliminate cellular debris, and engage in prolonged interactions with circulating lymphocytes due to their slow movement within the sinusoidal network. While KC are the dominant macrophage population in the liver under homeostatic conditions, they are not the only macrophages involved in hepatic immunity, other subsets also contribute significantly.

Those macrophages can polarize into distinct phenotypic states: the M1 phenotype, which is pro-inflammatory and promotes tissue damage while activating Th1 responses, and the M2 phenotype, which has anti-inflammatory properties, facilitates tissue repair, and activates

Th2 responses. Liver DC, derived from bone marrow precursors, play a crucial role in capturing and processing antigens for presentation to lymphocytes.

The innate lymphoid cell compartment includes NK cells and neutrophils, both of which patrol the liver and interact with sinusoidal endothelial cells to initiate immune responses. NK cells directly eliminate malignant or infected cells, leading to the clearance of these target cells. Meanwhile, neutrophils have a significant dual role in maintaining healthy liver conditions. On one hand, their infiltration contributes to immune defense through the release of cytokines, reactive oxygen species (ROS), and neutrophil extracellular traps (NETs), which trap and kill bacteria. However, the same mechanisms can also promote inflammation and tissue damage. On the other hand, recent studies propose that neutrophils help protect the liver by facilitating the resolution of tissue damage [18,34].

Unconventional T cell subsets, such as NKT cells, exhibit innate-like immune properties. These cells are characterized by the expression of NK cell markers. They respond to microbial and lipid antigens and can display both pro-inflammatory and anti-inflammatory effects, depending on the cytokine stimuli they receive [18,35,36].

Antigen-presenting cells (APCs) play a crucial role in initiating the adaptive immune response by processing and presenting antigens to T and B cells, the primary mediators of this response. In the hepatic sinusoids, B cells and T cells, including $CD4^+$ helper T cells and $CD8^+$ cytotoxic T cells, can be found. B cells produce antibodies, whereas T cells eliminate infected cells and help regulate immune activity through cytokine signaling. Among these, $CD8^+$ T cells are the most abundant subset in the liver, as they can differentiate into $CD8^+$ memory T cells. $CD4^+$ T cells, on the other hand, stimulate macrophages, B lymphocytes, and $CD8^+$ T cells.

In addition to APCs, HSC can also activate T cells. However, in a healthy liver, HSC typically remain in a quiescent state [18,34].

1.3.3. MODULATION OF THE HEPATIC IMMUNE SYSTEM IN MASH

MASH is increasingly recognized as an immune-mediated condition, not just a metabolic one. In patients with severe obesity, the disease begins with metabolic stress and insulin resistance, which promotes lipid accumulation in the liver and triggers chronic low-grade inflammation that disrupts both innate and adaptive immune responses. This activates liver-resident immune cells, particular KC, and recruits circulating monocytes that differentiate into inflammatory macrophages. These immune cells not only drive liver inflammation but also contribute to fibrosis through their interactions with hepatocytes and other non-parenchymal cells like HSC, which can be activated by KC and stimulate the collagen production.

Neutrophils, mainly recruited by KC, are the first to infiltrate the liver, further aggravating injury by releasing ROS and forming NETs, which can also activate HSC and promote tissue scarring. In the context of chronic liver inflammation, such as in MASH, the protective and reparative role of neutrophils becomes dysregulated, promoting tissue damage instead of resolution [18,36,37].

As MASH progresses, the number of DC increases. These DC mature into pro-inflammatory types, which then regulate the activity of NK cells and $CD8^+$ T cells. During persistent stress conditions, the function of NK cells becomes impaired, contributing to disease progression. Additionally, NKT cells are primarily exposed to a pro-inflammatory environment, which further exacerbates inflammation [32].

B and T cells are found to be elevated in MASH. B cells contribute to liver damage by secreting antibodies and B cell-activating factors, which promote inflammation and dysregulate T cells. $CD4^+$ T cells also play a significant role in liver damage by inducing apoptosis in hepatocytes, stimulating KC to adopt a pro-inflammatory phenotype, recruiting macrophages, and increasing lipid synthesis in the liver. Among $CD8^+$ T cells, the number of pro-inflammatory subsets increases, while Treg cells decrease, worsening the inflammatory response [18,32].

1.3.4.LIVER IMMUNE CHANGES IN WEIGHT-LOSS INDUCED MASH REMISSION

After bariatric surgery, changes in the immune system have been observed, particularly in association with reduced BMI and improvement in MASH. These changes may contribute to a reduction or even resolution of liver fibrosis. This is mainly due to a decrease in the release of pro-inflammatory cytokines by liver immune cells, which are inhibited and replaced by anti-inflammatory cytokines. The strengthening of the immune system following bariatric surgery enables immune cells to effectively continue their role in repairing liver damage [38,39].

Neutrophils are increasingly recognized as essential pro-resolving cells in liver inflammation. They control inflammation to prevent unwanted tissue damage and maintain tissue homeostasis. Upon undergoing apoptosis, they are engulfed by macrophages through a process known as efferocytosis, which in turn promotes macrophage polarization toward an M2 state. In this state, macrophages secrete anti-inflammatory cytokines and growth factors that aid in the degradation of extracellular matrix components and the resolution of fibrosis.

In addition to macrophages, CD8 T_{RM}, and NK contribute to the resolution by targeting and inducing apoptosis in HSC. The restoration of NK and NKT cells functionality following bariatric surgery further reinforces their protective role against fibrosis [40].

1.4.DIGITAL PATHOLOGY

Digital pathology (DP) is transforming histological image analysis by incorporating artificial intelligence (AI) into traditional histopathological workflows. Whole slide imaging enables high-resolution, real-time visualization of entire tissue sections, while deep learning algorithms facilitate automated pattern recognition and model training. This integration helps reduce inter-observer variability and provides quantitative, reproducible insights into disease progression, which is particularly valuable for evaluating and managing MASH [41].

Traditional scoring systems for MASH classification often lack sensitivity, and manual histological assessment can vary significantly [42]. Computer-aided image analysis addresses many limitations of these conventional approaches. The application of AI to

histopathological evaluations can enhance the recognition of key features, automate the quantification of cellular and structural components, and standardize analyses across large sample cohorts. This ultimately supports a more objective and scalable analysis.

An important tool in this field is QuPath, an open-source software developed for bioimage analysis [43]. QuPath allows users to annotate and interact with digitized histological slides as if they were viewed under a microscope, while also supporting the application and training of AI models [44]. In a typical workflow, pathologists first manually annotate digitized images to identify relevant histological features and to exclude artifacts from suboptimal staining or sample preparation. Next, image segmentation techniques are applied to generate predictions for each identified feature. Deep learning architectures, including convolutional neural networks and graph neural networks, are then used to classify and quantify histological readouts. This computational approach produces detailed, quantitative outputs that enhance our understanding of MASH [45].

2. HYPOTHESIS AND OBJECTIVES

Obesity is an increasing global concern characterized by the excessive accumulation of fat in the body. This condition can lead to a significant buildup of fat in the liver, resulting in MASLD and its more advanced form, MASH. Bariatric surgery, a common treatment for severe obesity, has been proven to cause substantial weight loss and improve both MASLD and MASH. Since recent research emphasizes that changes in the immune cell microenvironment are critical in the progression or resolution of MASH, **we hypothesize that there are significant changes in the number of immune cells in the liver before and after weight loss induced by bariatric surgery, which may be linked with improvements in liver damage.** Therefore, the main objective of this study is to evaluate the impact of bariatric surgery-induced weight loss on hepatic immune cell populations and their association with improvements in liver injury.

To adress this objective, we propose the following specific aims:

- To characterize the hepatic immune system environment in individuals with severe obesity both before and after surgery-induced weight loss.

- To examine the relationship between changes in immune cell infiltration after surgery and the improvement or worsening of Klainer's parameters and NAS, related to liver damage.

- To correlate the quantity of hepatic immune cell populations showing significant changes post-surgery with selected obesity-related comorbidities.

To achieve these objectives, we developed an AI-based method to quantify both the number and density of positive immune cells in immunohistochemistry (IHC) stains.

3. MATERIALS AND METHODS

3.1.STUDY DESIGN

This observational study, registered under ClinicalTrials.gov (ID: NCT05554224), involved collecting paired liver biopsy samples from 44 patients who underwent laparoscopic sleeve gastrectomy followed by a second bariatric surgery due to insufficient weight loss. The study was conducted at Hospital Universitari Sant Joan in Reus.

At the time of the initial surgery, all participants had a BMI between 35 and 40 kg/m² and presented high-risk comorbidities - including diagnosed or treated HTA, dyslipidemia, or T2DM - or had a BMI of 40 kg/m² or higher (*Table 3*). Only individuals aged 18 or older were included. Patients with clinical or laboratory signs of acute or chronic inflammation, infectious diseases, or cancer were excluded from the study.

The research adheres to the ethical principles outlined in the Declaration of Helsinki. Approval was granted by the Institutional Review Board under reference number EOMPI2024(244/2024) and informed consent was obtained from all participants.

3.2.SAMPLING

Liver biopsies were collected at the time of the interventions and preserved through formalin fixation, followed by paraffin embedding. Thin sections measuring 2 μm were cut using a microtome and mounted on slides for histological analysis. To evaluate steatosis, hepatocellular ballooning, lobular inflammation, and fibrosis, the samples were stained with H&E, as well as with Masson's Trichrome and IHC techniques (*Figure 5*). All tissue sections were initially deparaffinized before the staining procedures.

For H&E, sections were stained with hematoxylin to color the cell nuclei blue, followed by eosin, which stained the cytoplasm and extracellular matrix pink [46]. For Masson's Trichrome, sections were stained with a combination of dyes: the cytoplasm appeared red, while collagen fibers were stained blue or green, enabling the visualization of fibrosis [47]. Finally, for IHC, automated procedures were performed using Roche's BenchMark ULTRA

machine. Depending on the antibody, either the UltraView or OptiView detection kits were used. Detection was carried out with the DAB chromogen, and counterstaining was performed using hematoxylin. The detailed protocol for the process can be found in Supplementary Material.

After staining, the sections were dehydrated, cleared, and mounted for microscopic analysis.

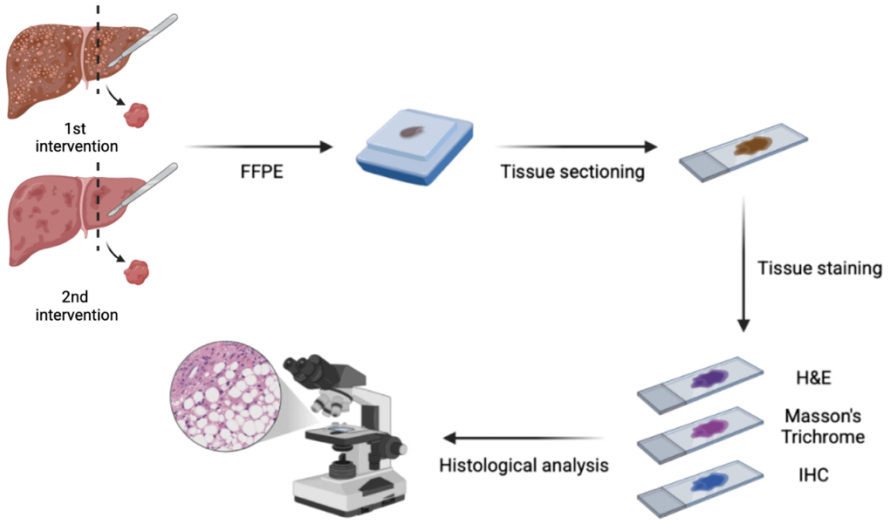

Figure 5. *Schematic representation of the liver biopsy sampling workflow. The histological image is stained with H&E and shown at 20x magnification. FFPE: formalin-fixation and paraffin embedding. Image created with BioRender.com.*

3.3.HISTOLOGICAL ANALYSIS

An expert hepatologist conducted the histological diagnosis of the samples using the *Kleiner* criteria [27]. The NAS was calculated by summing the individual scores for steatosis, hepatocellular ballooning and lobular inflammation. Patients were then categorized based on their NAS, and the distribution across the groups varied between the first and second intervention. For the non-MASH group, there was 1 patient in the first intervention and 27 patients in the second intervention. In the uncertain MASH group, there were 4 patients at the first intervention and 10 at the second intervention. Finally, in the MASH group, there were 39 patients at the first intervention and 7 at the second intervention (*Table 3*).

3.4.DIGITAL PATHOLOGY IMAGE ANALYSIS FOR IMMUNE CELL QUANTIFICATION

Following the initial assessment, the slides were scanned at 40X magnification using a Ventana DP 200 device (Roche, Basle, Switzerland). Image analysis was conducted using the QuPath software (Version 0.5.1). A project was created, and the whole slide images were imported. The default H-DAB filter was selected for the image type. To ensure accurate color representation, the "Estimate Stain Vectors" function was applied to each image, allowing for automatic color scale correction. Tissue annotations were created manually to delineate the regions of interest, categorizing them as tissue. To exclude non-representative or damaged peripheral areas, the "Expand Annotations" function was applied with an expansion radius of -100 μm. Any artifacts in the tissue were manually corrected by erasing them or adjusting the annotation region as necessary.

The "Positive Cell Detection" function was applied to all images to identify antibody-marked cells. During this process, the setup parameters were adjusted: the detection image parameter was set to "Optical Density Sum," and the requested pixel size was defined as 0.25 μm. All other parameters were left at their default settings except for the intensity threshold parameters. Specifically, the "Nucleus: DAB OD Mean" was manually adjusted based on the antibody used and the observed staining intensity through a trial-and-error approach (*Table 1*) (*Figure 6*).

Once all detections were completed, QuPath returned several parameters for each detected object, such as its coordinates, area, mean intensity, perimeter, and classification as positive or negative. Finally, the image-associated data was saved under the respective patient ID.

Table 1. *"Nucleus: BAB OD mean" threshold values for "Positive Cell Detection" function, categorized by antibody.*

TRESHOLD VALUES FOR "NUCLEUS: DAB OD MEAN"	
Antibody	Value
Anti-CD15	0.6
Anti-CD68	0.2
Anti-CD4	0.2
Anti-CD8	0.2
Anti-CD56	0.4
Anti-Gal3	0.1

3.5.DATA ANALYSIS AND STATISTICS

All statistical analyses were performed using R (version 4.4.2) in RStudio (version 2024.09.0.375).

The Shapiro–Wilk test was used to assess the normality of variable distributions, and Levene's test was applied to evaluate the homogeneity of variances. Quantitative variables were summarized using medians and interquartile ranges (IQRs), while categorical variables were presented as frequencies and percentages.

Given that most variables did not satisfy the assumptions of normality, non-parametric statistical methods were employed. The Wilcoxon rank-sum test was used for comparisons involving continuous variables, and the chi-squared test was used for categorical data. For comparisons across more than two groups, the Kruskal–Wallis test was applied.

All R scripts used for statistical analyses are provided in the Supplementary Material. Graphical outputs were refined using Inkscape software to improve visual quality [48].

3.5.1.CHARACTERIZATION OF THE HEPATIC IMMUNE SYSTEM ENVIRONMENT IN INDIVIDUALS WITH SEVERE OBESITY BOTH BEFORE AND AFTER SURGERY-INDUCED WEIGHT LOSS

Data from each slide, obtained from QuPath, was imported into RStudio and combined into a single dataset. To enhance data quality, the dataset was filtered to exclude certain objects, thereby reducing the occurrence of false positive and false negative detection of cells. To address false positives, only positive cells with an area exceeding the minimum threshold

defined for each specific cell type were retained. This area threshold varied by cell type, as detailed in *Table 2*, and was determined based on scientific literature. For false negatives, the dataset included only objects with an H-DAB staining intensity of at least 0.05. This staining intensity threshold was consistently applied across all markers since the staining procedure was uniform (*Figure 6*).

After filtering, objects were grouped by image ID, and the number of positive and negative cells was counted. The proportion of positive cells per image was then calculated (positive cells / (positive cells + negative cells)) and incorporated into the dataset. To determine the density of positive cells (positive cells/mm²), the total area of all objects in each image was summed and converted to mm².

A final Excel file was generated, containing only the relevant objects and computed values.

A Wilcoxon test was performed on the positive cell count and cell density to assess whether the changes between the first and second interventions were statistically significant.

Table 2. *Minimum area threshold value for positive cell selection, categorized by immune cell type [49–53]*

TRESHOLD VALUES FOR "CELL: MINIMUM AREA"		
Antigen	**Value (μm²)**	**Author (year)**
CD15	110	Tigner et al. (2025)
CD68	16	Donadon et al. (2020)
CD4	50	Wang et al. (2014)
CD8	95	Howden et al. (2019)
CD56	28	Dickinson et al. (2015)
Gal3	-	-

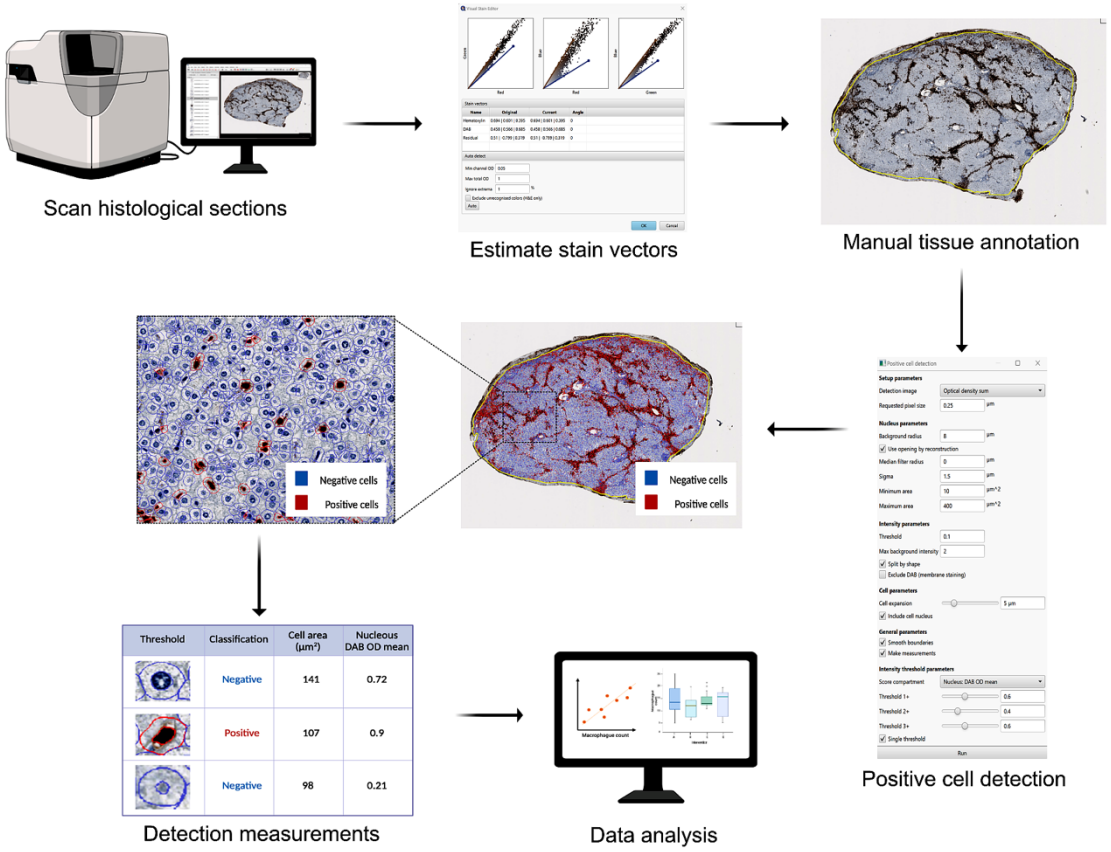

Figure 6. Representation of the methodology for developing digital pathology image analysis. *Histological images were stained using IHC and visualized at 20× magnification for the zoomed-in view and at 3× magnification for the two distant views. Image created with BioRender.com.*

3.5.2.EXPLORING THE RELATIONSHIP BETWEEN CHANGES IN IMMUNE CELL INFILTRATION AFTER SURGERY AND THE IMPROVEMENT OR WORSENING OF LIVER DAMAGE PARAMETERS

Based on the clinical information collected from each patient, including liver damage parameters such as the Kleiner scores (ballooning score, inflammation score, fibrosis score, and steatosis score) and the NAS from both interventions, the variation in each parameter was calculated (2nd intervention – 1st intervention). This provided a numerical assessment of whether liver damage had worsened or improved following surgery, as well as the degree of change for each parameter. The variations in cell count and density between the two interventions were calculated in a similar manner. As a result, a comprehensive Excel database was generated, containing the calculated differences for the Kleiner parameters, NAS, positive cell count, and positive cell density.

Statistical comparisons were made using the Kruskal-Wallis test to assess global differences between groups, followed by pairwise comparisons using the Wilcoxon test for each pair of levels within the categorical variable.

3.5.3. THE IMPACT OF COMMORBIDITIES ON HEPATIC IMMUNE SYSTEM

A different Excel database was generated to explore the potential associations between the proportion and density of CD15-positive cells and the presence of three obesity-related comorbidities identified during clinical characterization: T2DM, HTA, and dyslipidemia. For each patient, the dataset included values for the proportion and density of CD15-positive cells observed at the first intervention, along with binary indicators indicating presence or absence of each comorbidity.

Statistical differences between the groups were assessed using the Wilcoxon test.

4. RESULTS

4.1.BARIATRIC SURGERY IMPROVES METABOLIC PARAMETERS AND LIVER HEALTH IN PATIENTS WITH SEVERE OBESITY

As shown in *Table 3*, the majority of patients in this study were women. As anticipated, patients in the 2nd intervention were significantly older than in the 1st intervention, with a *p*-value of 0.02. Additionally, the median BMI was notably higher in the 1st intervention (52.4 kg/m^2) compared to the 2nd (40.7 kg/m^2), with a *p*-value of $6.05x10^{-13}$.

Concerning obesity-associated comorbidities, a substantial number of patients presented at least one condition. However, significant differences between interventions were observed only in the prevalence of T2DM, which was more frequent in the 1st intervention, with a *p*-value of $6.93x10^{-3}$. No significant differences were noted for dyslipidemia or HTA.

The distribution of NAS categories varied significantly between interventions. While most patients in the 1st intervention were diagnosed with MASH, the 2nd intervention had a significantly higher proportion of non-MASH cases, with a *p*-value of $2.32x10^{-11}$. A small percentage of patients remained in the uncertain MASH category (*Figure 7*).

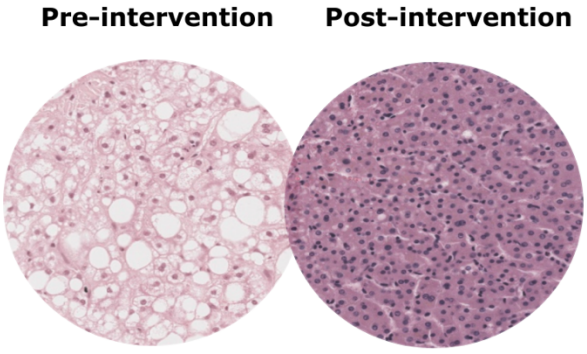

Figure 7. Illustration showing histological improvement of liver tissue following bariatric surgery. *Representative H&E-stained liver sections from the same patient before and after bariatric surgery, visualized at 10× magnification. Image created with InkScape.*

Liver damage parameters also differed between interventions. In the 2nd intervention, patients exhibited less severe steatosis, with most of them having less than 5% steatosis (*p*-

value of 9.49×10^{-9}**).** In contrast, higher grades of steatosis were more prevalent in the 1st intervention. Hepatocellular ballooning displayed notable differences as well: a greater number of patients in the 2nd intervention presented no ballooning, while in the 1st intervention, patients had multiple ballooned cells (*p*-value of 1.66×10^{-6}).

In terms of lobular inflammation, the distribution of inflammatory foci was similar between the groups, with no significant differences noted. However, fibrosis stages exhibited some variation. A higher prevalence of perisinusoidal and periportal fibrosis (F2) was observed in the 2nd intervention, whereas bridging fibrosis (F3) was more frequent in the 1st intervention. Cirrhosis was rare and similarly distributed between the two groups.

Table 3. Clinical characterization of the patients. *Qualitative variables are presented as n (%), and quantitative variables as median [interquartile range]. Statistically significant differences are indicated in bold.*

	1st intervention	2nd intervention	*p*-value
Women, n (%)	36 (81.8%)	36 (81.8%)	N/A
Age, years	44 [39-49]	49 [43-57]	0.02
BMI, kg/m^2	52.4 [47.2-57.7]	40.7 [37.0-43.0]	**6.05×10^{-13}**
Comorbidities			
T2DM (%)	14 (31.8)	3 (6.8)	**6.93×10^{-3}**
Dyslipidemia (%)	14 (31.8)	7 (15.9)	0.13
HTA (%)	19 (43.2)	10 (22.7)	0.07
NAS diagnosis (%)			
MASH	39 (88.6)	7 (15.9)	
Non-MASH	1 (2.3)	27 (61.4)	
Uncertain	4 (9.1)	10 (22.7)	**2.32×10^{-11}**
Liver damage parameters			
Steatosis grade, n (%)			
<5%	7 (15.9)	35 (79.5)	
5–33%	19 (43.2)	9 (20.5)	
> 33–66%	13 (29.5)	0	
> 66%	5 (11.4)	0	**9.49×10^{-9}**
Hepatocellular ballooning, n (%)			
No	2 (4.5)	21 (47.7)	
Few cells	11 (25.0)	13 (29.5)	
Many cells	31 (70.5)	10 (22.7)	**1.66×10^{-6}**
Lobular inflammation, n (%)			
No foci	0	0	

< 2 foci	1 (2.3)	3 (6.8)	
2-4 foci	24 (54.5)	21 (47.7)	
> 4 foci	19 (43.2)	20 (45.5)	0.54
Fibrosis, n (%)			
None (F0)	0	0	
Perisinusoidal or periportal (F1)	0	4 (9.1)	
Perisinusoidal and periportal (F2)	21 (47.7)	26 (59.1)	
Bridging fibrosis (F3)	22 (50.0)	13 (29.5)	
Cirhosis (F4)	1 (2.3)	1 (2.3)	0.08

4.2.SURGERY-INDUCED WEIGHT LOSS MODIFIES THE HEPATIC IMMUNE LANDSCAPE

The profiles of innate immune cells in patients with severe obesity were evaluated before and after surgery-induced weight loss, as illustrated in *Figure 8*. Following the surgery, there was a significant increase in both the proportion and density of CD15-positive cells, which primarily indicate neutrophils. The *p*-values for these findings were 3.71×10^{-6} and 5.26×10^{-6}, respectively. CD68-positive cells, which are markers for macrophages, showed only a slight increase after surgery that was not statistically significant (*p*-value of 0.08 for proportion and 0.11 for density). Similarly, CD56-positive cells, which identify NK cells, also exhibited a non-significant increase compared to the first intervention levels (*p*-value of 0.53 for proportion and 0.49 for density) (*Table S1*).

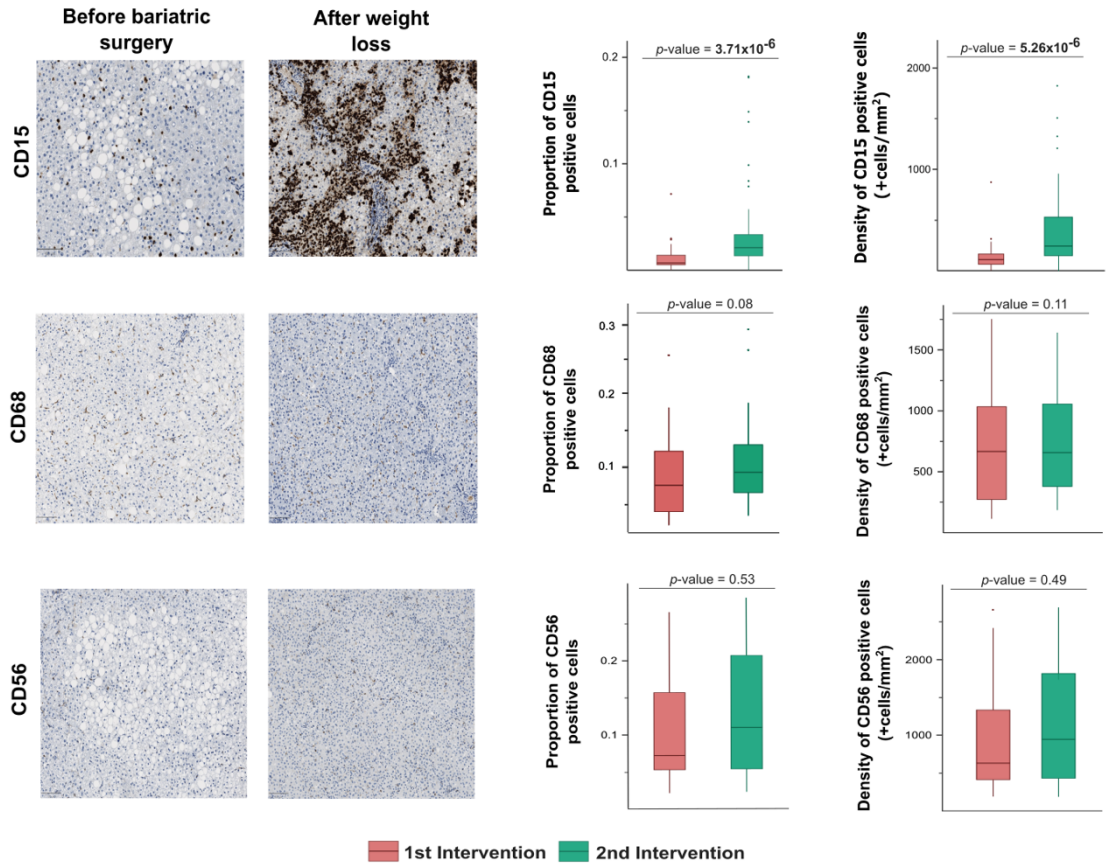

Figure 8. Comparison of innate immune cell profiles in MASH patients before and after surgery-induced weight loss. *Histological sections were stained using IHC and visualized at 10x magnification. Graphics on the left compare the proportion of positive cells between interventions, while graphics on the right compare their density. Statistically significant differences are indicated in bold.*

Figure 9 illustrates the profiles of adaptive immune cells in our cohort before and after weight loss induced by surgery. The analysis showed a decrease in both the proportion and density of CD8-positive cells after surgery compared to pre-surgery levels; however, this reduction was not statistically significant, with *p*-values of 0.74 and 0.31, respectively. In contrast, the number of CD4-positive cells increased, but this change also did not reach statistical significance, with *p*-values of 0.12 for proportion and 0.05 for density.

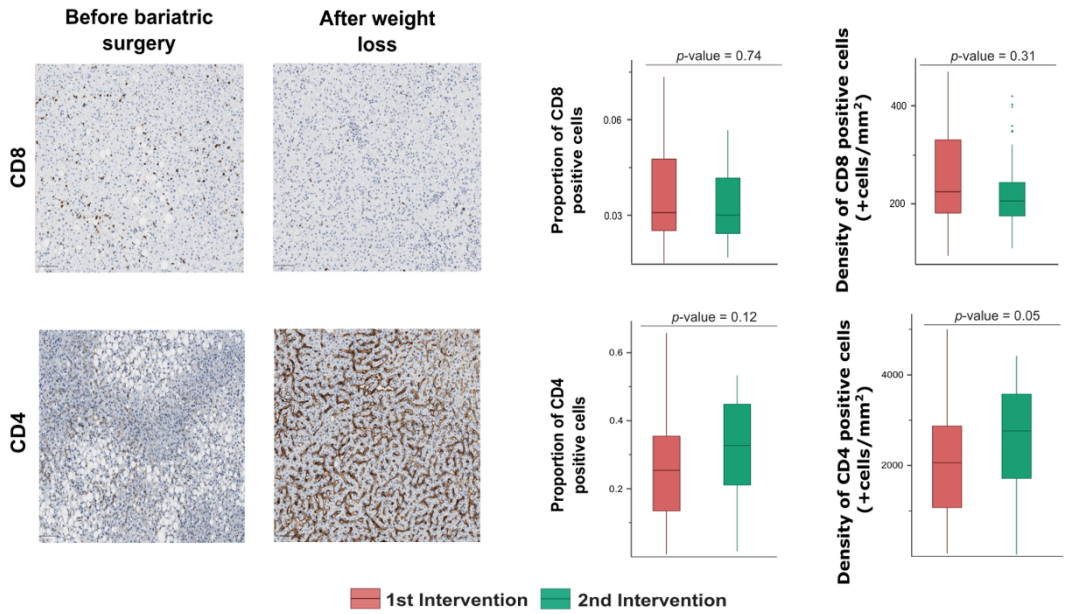

Figure 9. Comparison of adaptive immune cell profiles in MASH patients before and after surgery-induced weight loss. *Histological sections were stained using IHC and visualized at 10x magnification. Graphics on the left compare the proportion of positive cells between interventions, while graphics on the right compare their density.*

Furthermore, the expression of Gal3, a marker associated with inflammation (*Table S1*), was assessed, as illustrated in *Figure 10.* Although there was a trend toward a decrease in the number of Gal3-positive cells following surgery-induced weight loss, this change did not achieve statistical significance, with *p*-values of 0.88 for proportion and 0.91 for density.

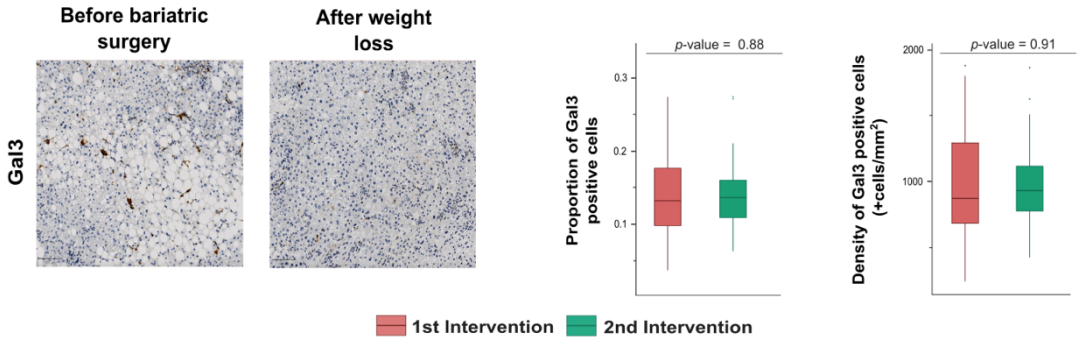

Figure 10. Comparison of inflammatory profiles in MASH patients before and after surgery-induced weight loss. *Histological sections were stained using IHC and visualized at 10x magnification. Graphics on the left compare the proportion of positive cells between interventions, while graphics on the right compare their density.*

4.3.CHANGES IN IMMUNE CELL INFILTRATION FOLLOWING SURGERY-INDUCED WEIGHT LOSS ARE ASSOCIATED WITH IMPROVED LIVER DAMAGE PARAMETERS

Regarding innate immune cells, both the proportion of CD15-positive cells and their density showed a significant increase from the first intervention to the second, as seen in *Figure 8*. However, when we analyzed their behavior in relation to the Kleiner scores and the NAS, neither the cell count nor the cell density demonstrated a clear pattern of change, as illustrated in *Figure 11*.

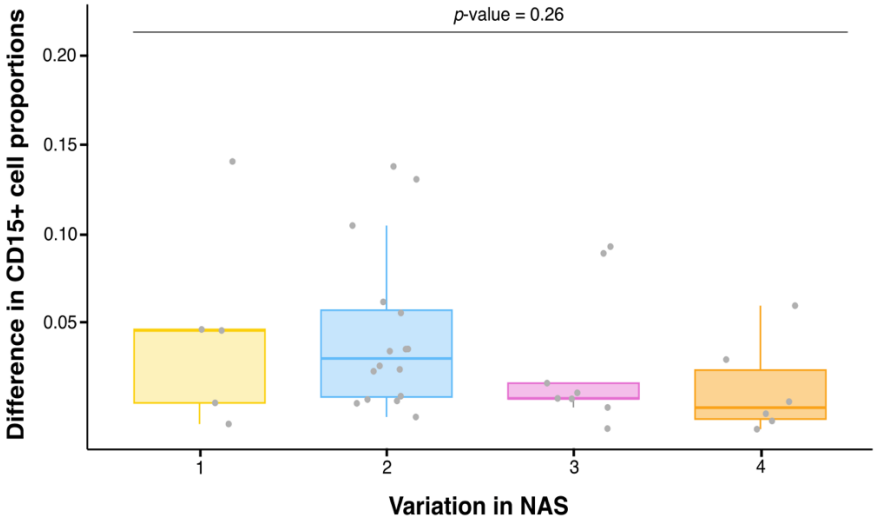

Figure 11. Association between the variation in NAS and the difference in CD15-positive cells proportions. *The boxplot illustrates the differences in CD15-positive cell proportion between the second and first interventions across the different degrees of NAS variation. A variation value of 1 indicates a reduction of one grade in the NAS between interventions, 2 indicates a reduction of two grades, and so on.*

CD68-positive cell count and density exhibited a slight, non-significant increase between the first and second intervention (*Figure 8*). Nevertheless, as illustrated in *Figure 12*, significant associations were found between changes in CD68-positive cells proportion and density and the variation in both the ballooning score and the NAS.

In particular, regarding the link between the difference in CD68-positive cells proportion and the variation in ballooning score (*Figure 12A*), the overall relation was not statistically significant (*p*-value = 0.08). However, a notable difference was detected between patients with a variation of 0 grades and those with a variation of 2 grades (*p*-value = 0.04).

Similarly, for alterations in CD68-positive cells density in relation to ballooning score variation (*Figure 12C*), the global association did not reach significance (*p*-value = 0.05). Even so, a statistically significant difference was found between patients with an improvement of 0 grades and those with a variation of 2 grades (*p*-value = 0.03).

As for the relationship between the difference in CD68-positive cells proportion and the variation in NAS (*Figure 12B*), a significant overall association was identified (*p*-value = 0.02). Pairwise comparisons revealed significant differences between the variation of 1 grade and 2 grades (*p*-value = 0.03), 1 grade and 3 grades (*p*-value = 0.01), and 1 grade and 4 grades (*p*-value = 0.02).

A significant global association was observed between the difference in CD68-positive cell density and the variation in NAS, as shown in *Figure 12D* (*p*-value = 0.01). Statistically significant differences were found when comparing 1-grade variation with 2, 3, and 4 grades, with a *p*-value of 0.01 for all of them.

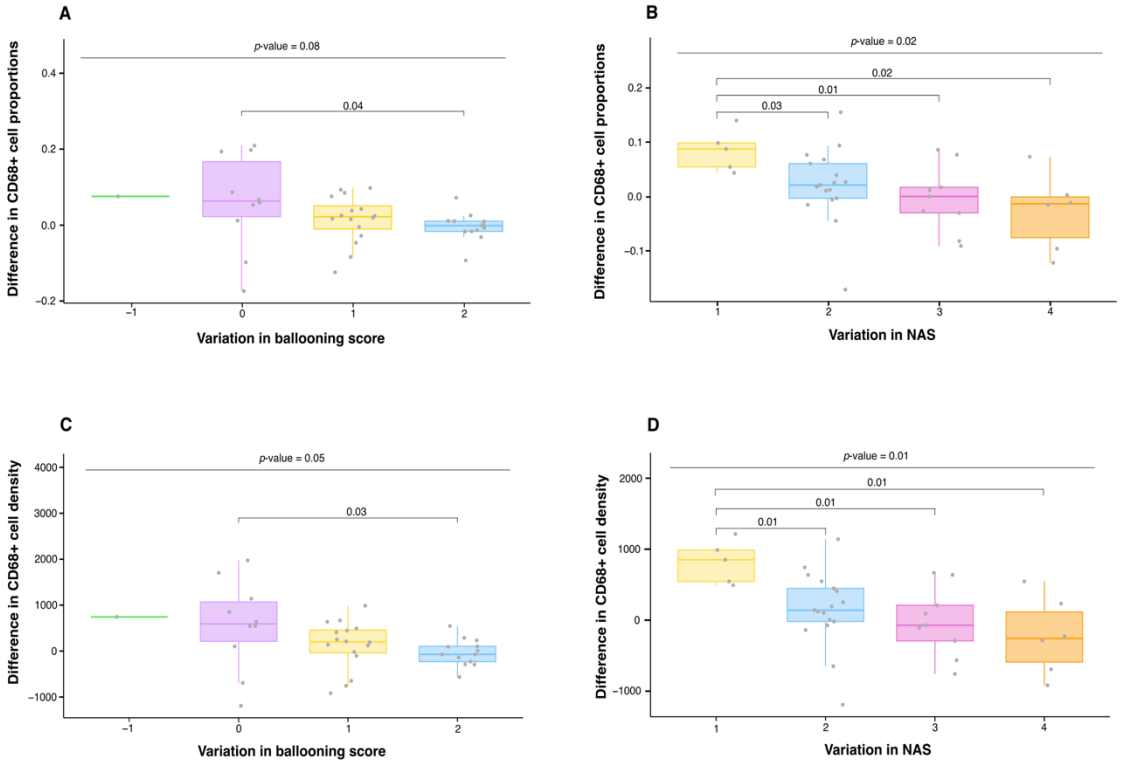

Figure 12. Association between the variation in ballooning score and NAS, and the difference in CD68-positive cells proportion and density. *Panels (A, C) show the association between the variation in ballooning score and the difference in CD68-positive cells proportion (A) and density (C) between interventions. Panels (B, D) show the association between the variation in NAS and the difference in CD68-*

positive cells proportion (B) and density (D) between interventions. A variation value of 1 indicates a reduction of one grade in the Kleiner parameter score between interventions, 2 indicates a reduction of two grades, and so on.

The proportion and density of CD56-positive cells exhibited a non-significant increase between the first and second intervention (*Figure 8*). When examining their relationship with the Kleiner scores and the NAS, nor the cell count or cell density did not show a consistent pattern of change (*p*-value of 0.47 for NAS), as illustrated in *Figure 13*.

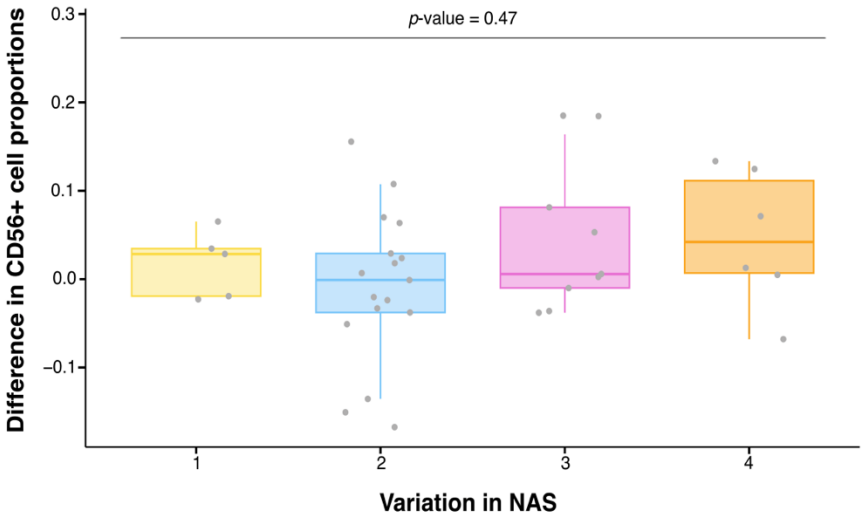

Figure 13. Association between the variation in NAS and the difference in CD56-positive cells proportion. *The boxplot illustrates the differences in CD56-positive celsl proportion between the second and first intervention across the different degrees of NAS variation. A variation value of 1 indicates a reduction of one grade in the NAS between interventions, 2 indicates a reduction of two grades, and so on.*

Moving on to adaptive immune cells, the proportion of CD8-positive cells showed a decrease from the first to the second intervention, although this change was not statistically significant (*Figure 9*). Regarding the difference in CD8-positive cells proportion and density between interventions, no significant relations were found with any of the Kleiner parameters or with the NAS (*p*-value of 1.00 for NAS) (*Figure 14*).

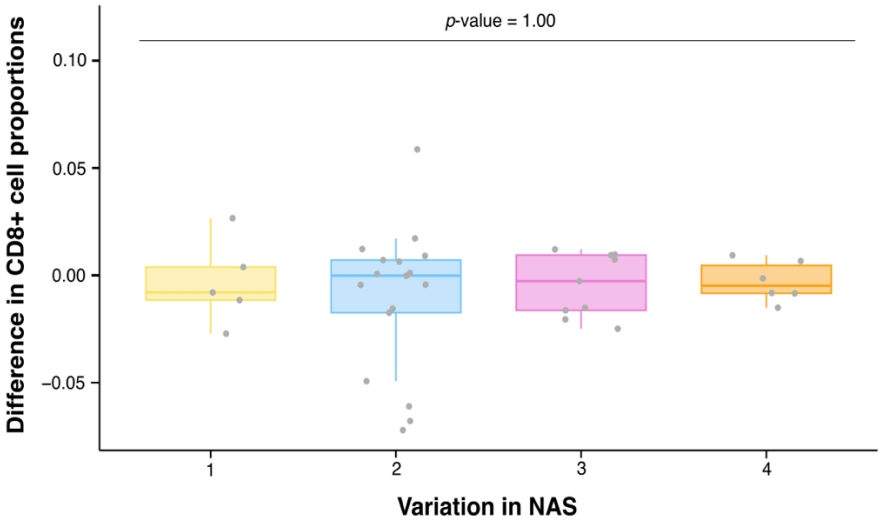

Figure 14. Association between the variation in NAS and the difference in CD8-positive cells proportion. *The boxplot illustrates the differences in CD8-positive cells proportion between the second and first intervention across the different degrees of NAS variation. A variation value of 1 indicates a reduction of one grade in the NAS between interventions, 2 indicates a reduction of two grades, and so on.*

The tendency of the proportion of CD4-positive cells was to increase after surgery, although this change was not statistically significant (*Figure 9*). As illustrated in *Figure 15A*, the change in CD4-positive cells proportion between the interventions did not show a significant association with the overall variation in the steatosis score. However, a significant difference was observed when comparing variations of 0 grades and 3 grades (*p*-value = 0.03). Additionally, no significant association was found with the NAS variation (*Figure 15B*). Furthermore, there were no significant relations detected between the difference in CD4-positive cells density and any of the Kleiner parameters or the NAS.

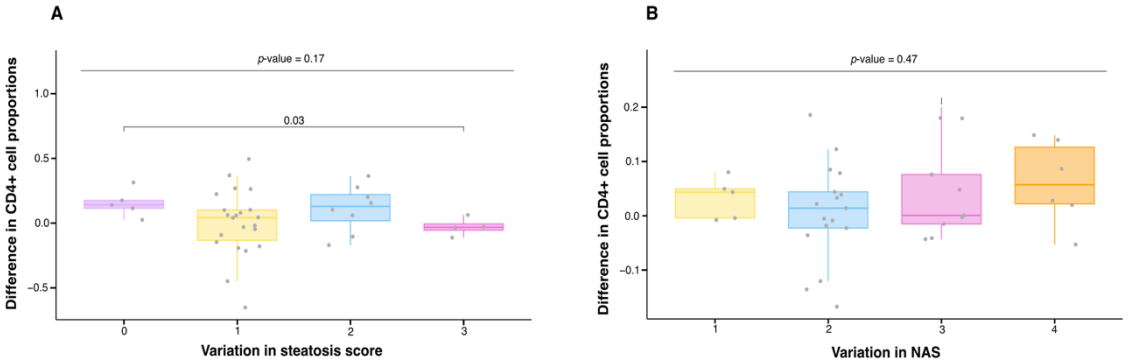

Figure 15. Association between the variation in steatosis score and NAS, and the difference in CD4-positive cells proportion and density. *Panel (A) shows the association between the variation in steatosis score and the difference in CD4-positive cells proportion between interventions. Panel (B) shows the association between the variation in NAS and the difference in CD4-positive cells proportion between interventions. A variation value of 1 indicates an increase of one grade in the Kleiner parameter score between interventions, 2 indicates an increase of two grades, and so on.*

Regarding the inflammatory marker Galectin-3, the proportion of positive cells decreased after the intervention (*Figure 10*). Overall, there were no statistically significant associations between changes in Gal3-positive cells proportion or density and any of the Kleiner parameters. However, when analyzed by differences in ballooning scores, a significant association was found between variations of 0 grades and 1 grade, with *p*-values of 0.04 for both cell count (Figure 16A) and cell density (Figure 16C).

For the NAS, not overall statistically significant differences were detected. Nevertheless, specific comparisons revealed significant findings between variations of 1 grade and 4 grades, with *p*-values of 0.03 for both cell count (Figure 16B) and density (Figure 16D). Additionally, a significant change was observed between variations of 2 grades and 4 grades between interventions in terms of cell count (Figure 16B), with a *p*-value of 0.04.

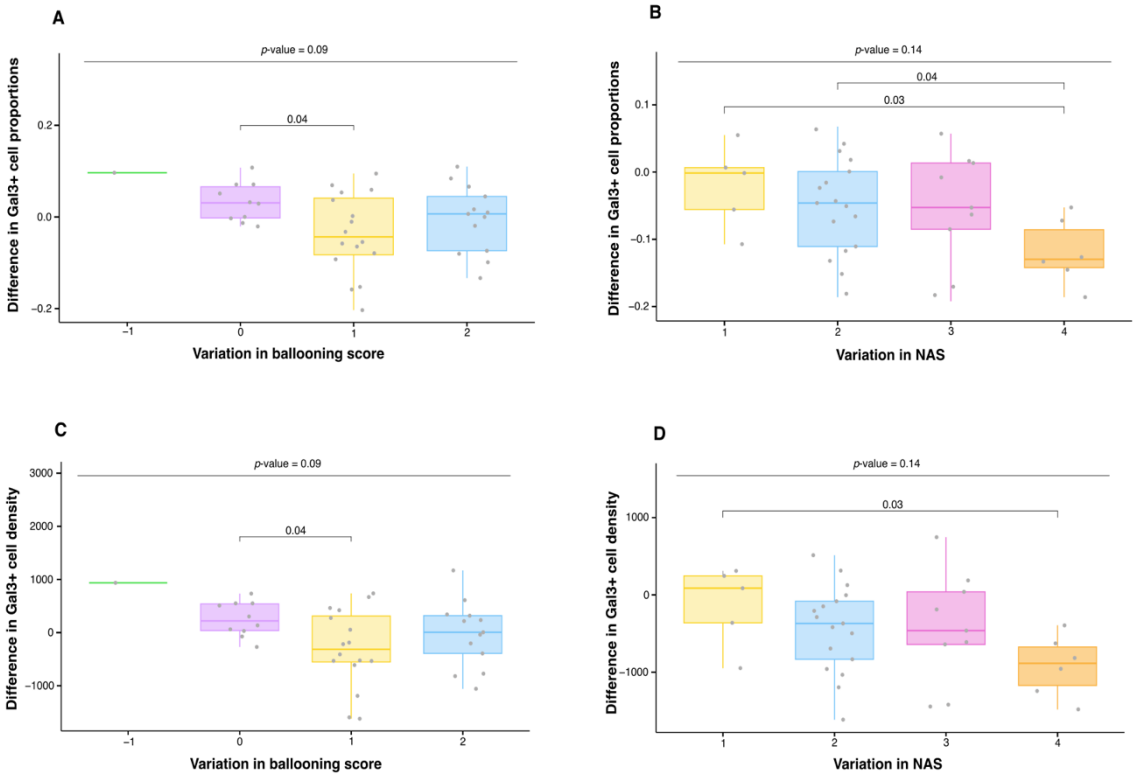

Figure 16. Association between the variation in ballooning score and NAS, and the difference in Gal3-positive cells proportion and density. *Panels (A, C) show the association between the variation in ballooning score and the difference in Gal3-positive cells proportion (A) and density (C) between interventions. Panels (B, D) show the association between the variation in NAS and the difference in Gal3-positive cell proportions (B) and density (D) between interventions. A variation value of 1 indicates an increase of one grade in the Kleiner parameter score between interventions, 2 indicates an increase of two grades, and so on.*

4.4. IMPACT OF T2DM, HTA, AND DYSLIPIDEMIA ON CD15+ CELL PROPORTION AND DENSITY IS NOT SIGNIFICANT

To explore potential associations between hepatic CD15-positive cells populations and the presence of obesity-related comorbidities at the time of the first surgical intervention, we compared both the proportion and density of CD15-positive cells in patients stratified by comorbidity status.

As shown in *Figure 17*, no statistically significant differences were observed in the proportion (*Figure 17A*) or density (*Figure 17B*) of CD15-positive cells between patients with and without T2DM (*p*-value of 0.52 for both proportion and density).

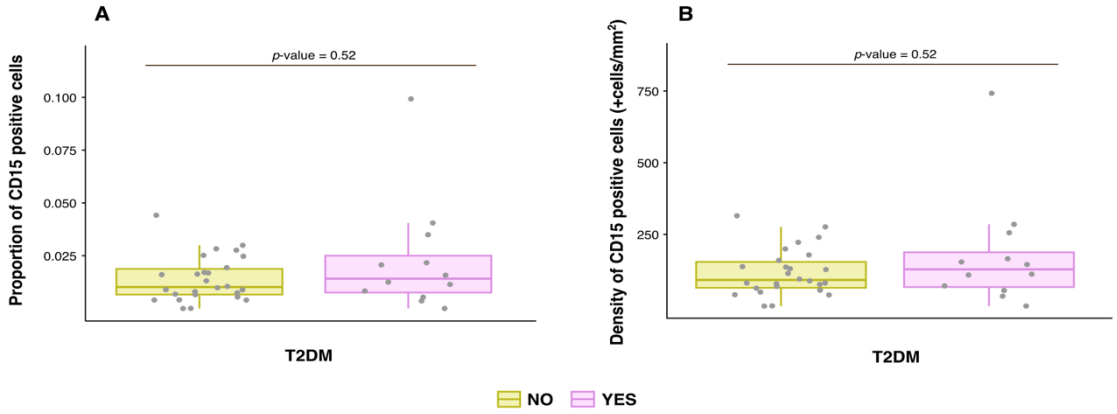

Figure 17. Relationship between the proportion and density of CD15-positive cells and the presence or absence of T2DM, at the first intervention. *(A) Shows the relationship between the proportion of CD15-positive cells and the presence or absence of T2DM. (B) Shows the relationship between the density of CD15-positive cells (+cells/mm²) and the presence or absence of T2DM.*

Similarly, comparisons based on the presence of HTA revealed no significant differences, as seen in *Figure 18 A and B,* with a *p*-value of 0.58 for the proportion and 0.73 for the density.

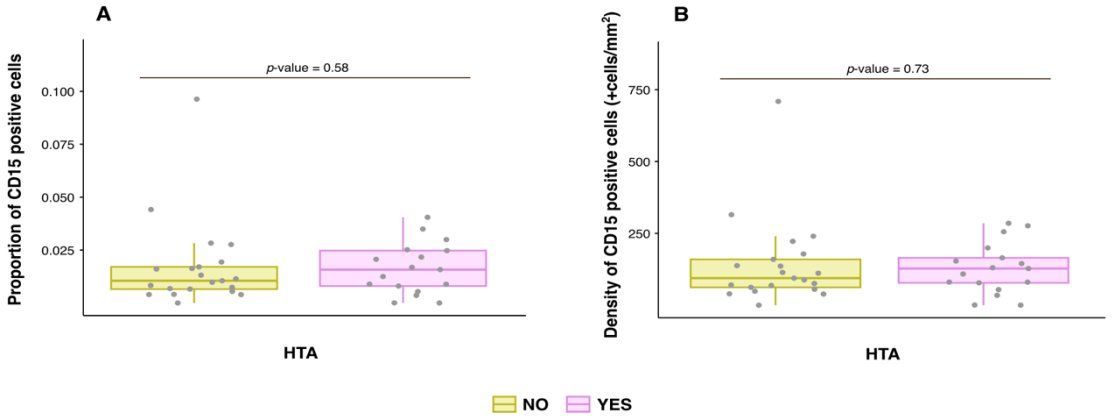

Figure 18. Relationship between the proportion and density of CD15-positive cells and the presence or absence of HTA, at the first intervention. *Panel (A) shows the relationship between the proportion of CD15-positive cells and the presence or absence of HTA. Panel (B) shows the relationship between the density of CD15-positive cells (+cells/mm²) and the presence or absence of HTA.*

Lastly, the analysis of dyslipidemia status also showed no significant differences in CD15-positive cells populations (*Figure 19*) (*p*-value of 0.59 for proportion and 0.48 for density).

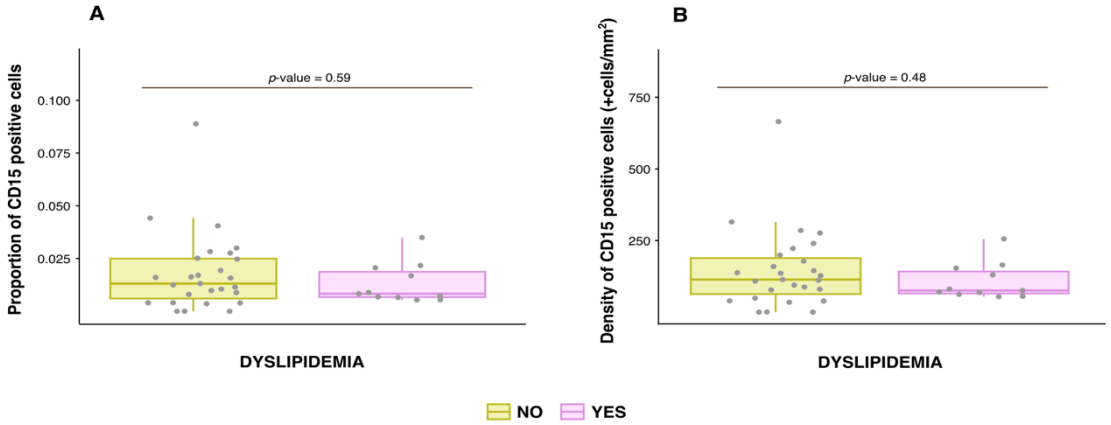

Figure 19. Relationship between the proportion and density of CD15-positive cells and the presence or absence of dyslipidemia, at the time of the first intervention. *Panel (A) shows the relationship between the proportion of CD15-positive cells and the presence or absence of dyslipidemia. Panel (B) shows the relationship between the density of CD15-positive cells (+cells/mm²) and the presence or absence of dyslipidemia.*

5. DISCUSSION

Obesity is a metabolic disorder that has significantly increased worldwide over recent decades [54]. People with severe obesity face a higher risk of premature death and typically suffer from multiple comorbidities that reduce quality of life [55]. To date, bariatric surgery has been the most effective treatment for severe obesity and its associated conditions [56].

In these patients, excess TAG accumulation in the liver leads to steatosis, which may progress to MASLD and eventually MASH if untreated [57]. In MASH, liver dysfunction and metabolic imbalance create a pro-inflammatory environment both locally and systemically, driving disease progression. Increasing evidence shows that bariatric surgery improves - and may even resolve - MASH [58]. This has been linked to immune system remodeling, not only in the liver but also systemically [59].
Therefore, our objective was to evaluate the impact of bariatric surgery-induced weight loss on hepatic immune cell populations and their associations with improvements in liver damage.

In our cohort, we evaluated clinical parameters before and after sleeve gastrectomy and observed expected improvements [60]. BMI decreased significantly, and parameters of liver damage improved. Although the surgery promotes weight loss and improves metabolic health, weight regain and insufficient weight loss remain a common concern [61]. This occurred in our cohort, requiring a second procedure [62]. This allowed us to collect two liver biopsies per patient and analyze the impact of surgery on liver damage.

To explore immune changes, we used digital pathology to quantify immune cell subtypes in liver samples. Traditionally histopathology relies on manual counting by pathologists, a subjective method prone to variability. Inter- and intra-observer differences can bias results and limit reproducibility, especially when detecting slight changes in cell numbers or distribution [45]. Digital pathology offers a more objective and consistent alternative. It reduces variability and enables accurate automated quantification [63]. For this study, we used QuPath, an open-source digital pathology platform intended for research use only, to

analyze immune cells stained with antibodies (anti-CD15, CD68, CD56, CD4, CD8, and Galectin-3), to detect changes in their proportion and density before and after bariatric surgery [64].

Interestingly, we found a significant increase in CD15+ cells, primarily neutrophils, after bariatric surgery. This may seem unexpected since neutrophils are commonly associated with MASH progression due to their release of excessive ROS, proteolytic enzymes, and pro-inflammatory cytokines. These actions disrupt immune balance and worsen liver injury [65]. However, emerging data reveal a dual role for neutrophils. After bariatric surgery – when inflammation resolves - they may regain regulatory and reparative functions [66]. Several mechanisms could explain this shift. Neutrophil heterogeneity allows for distinct subsets with different inflammatory roles depending on context [67]. Also, matrix metalloproteinases (MMPs) released during neutrophil extravasation can degrade fibrotic tissue and promote healing, although they can also stimulate fibrogenesis, highlighting a delicate balance. Additionally, microRNA-223, the most abundant microRNA in neutrophils, modulates neutrophil and macrophage activity, preventing excessive immune responses. This promotes a shift in macrophages from the classically activated M1 pro-inflammatory phenotype, toward an alternatively activated M2 anti-inflammatory phenotype [68,69]. Efferocytosis – the engulfment of apoptotic neutrophils by macrophages – further promotes M2 polarization and resolution of inflammation [70]. Therefore, the rise in CD15+ cells after surgery may reflect a reparative immune response, not pathological activation.

In line with this hypothesis, although total $CD68^+$ macrophage levels remained stable, patients with improved ballooning and NAS had significant reductions in these cells. This suggests region-specific immune remodeling during liver recovery. Since CD68 is a general macrophage marker that does not distinguish between pro-inflammatory (M1) and anti-inflammatory (M2) types, stable total counts may mask underlying shifts in macrophage phenotype [71]. In areas undergoing repair, macrophages may either decrease due to reduced inflammatory signaling or shift from M1 to M2. This change cannot be detected with CD68 – specific markers like CD86 (M1) and CD206 (M2) are needed for phenotyping [72,73].

This interpretation is supported by our findings on Gal-3, a lectin that promotes inflammation and fibrosis [74–76]. Although overall Gal3+ cell levels did not change significantly across the cohort, patients with histological improvement - especially in ballooning and NAS - had significant local reductions in Gal3+ cells. This suggests that Gal-3 expression may decrease specifically in regenerating areas, due to reduced inflammatory signaling in a healing liver.

Similarly, we observed a non-significant increase in CD4+ T cells after surgery; however, there was a significant rise in those patients who experienced improved steatosis. Among CD4+ T cells, Tregs are known for their anti-inflammatory function and support of tissue repair. Some studies indicate that CD4+ Tregs are reduced in individuals with obesity but increase after bariatric surgery [77,78]. Although we did not identify specific CD4+ cell subsets in our study, our findings suggest that Tregs may play a role in the observed improvements.

Finally, we found no link between baseline CD15+ cell levels and metabolic comorbidities. This suggests that obesity-related conditions are unlikely to be confounding factors in our evaluation of CD15+ cell dynamics and that the immune shifts observed are likely due to the effects of surgery itself, rather than pre-existing conditions [79].

6. CONCLUSION

The main conclusions derived from this study are the following:

Regading the first objective, which aimed to characterize the hepatic immune environment in individuals with severe obesity before and after surgery-induced weight loss:

- After bariatric surgery, the composition of immune cell populations in the liver undergoes several alterations. Among all the cell types analyzed, only $CD15^+$ cells showed a statistically significant increase post-surgery, suggesting a potential involvement of neutrophils in tissue repair processes in the liver.

For the second objective, which focused on examining the relationship between changes in immune cell infiltration and the improvement of liver damage parameters:

- Immune remodeling following weight loss showed an association with histological improvements in MASH.
  - Macrophages may undergo phenotypic polarization toward an anti-inflammatory (M2) state, potentially supporting tissue repair.
  - $CD4^+$ T cells, especially $CD4^+$ Tregs, may actively participate in resolving inflammation, consistent with their known immunomodulatory functions.
  - Overall, the improvement in liver injury appears to be associated with a reduction in the pro-inflammatory immune state following surgery.

Concerning the third objective, which explored correlations between the quantity of immune cells with significant post-surgical changes and obesity-related comorbidities:

- The post-surgical immune changes observed are not influenced by pre-existing conditions, such as obesity-related comorbidities.

Therefore, this study provides quantitative evidence that bariatric surgery is associated with immune remodeling in the liver, alongside histological improvements in MASH. While causality cannot be established, these findings support the notion that immune shifts may contribute to the resolution process. Moreover, digital pathology sets a methodological precedent for future investigations into immune-mediated mechanisms of liver repair.

7. LIMITATIONS AND FUTURE PERSPECTIVES

Our study provides new insights into how bariatric surgery modifies the hepatic immune landscape in patients with severe obesity and contributes to MASH resolution. However, several limitations should be considered:

1. The small cohort size limits generalizability, and the observational design prevents establishing causality between bariatric surgery and the immune changes observed.

2. It remains possible that the immune changes are a secondary consequence of the improvements induced by the intervention rather than being directly responsible for MASH resolution.

3. Clinical metrics such as NAS and BMI, though widely used, may not fully capture disease complexity or body composition.

4. The use of CD68 as a general macrophage marker also limited our ability to assess polarization; future studies should include markers like CD86 and CD206.

5. Since we did not identify specific CD4+ T cells subtypes, future studies should characterize $CD4^+$ subsets to clarify their role in liver repair.

6. While digital pathology was used for quantifying immune cells, the initial diagnostic classification of liver biopsies was conducted using conventional microscopy. Implementing digital pathology in all histological assessments could enhance consistency and decrease variability related to observers.

7. Our analyses focused on the overall quantification of immune cells without considering potential spatial variations in their distribution. Future studies should investigate whether immune cells relocate after surgery is associated with disease resolution.

ACKNOWLEDGMENTS

Vull agrair sincerament al Prof. Joven per haver-me donat l'oportunitat de formar part del seu equip d'investigació durant la meva estada. Ha estat una experiència inestimable per al meu creixement acadèmic i personal.

Un agraïment molt especial a la meva supervisora de projecte, Alina Iuliana Onoiu. La teva inspiració, el teu coneixement i la teva guia han estat fonamentals al llarg de tot el procés.

També vull mostrar el meu profund agraïment al meu tutor acadèmic, Antonio Jesús Cortés Espinar, pel seu suport constant i la seva ajuda al llarg del projecte.

Al Ferran, per sempre fer-me sentir recolzada en tots els àmbits de la meva vida.

Als meus avis, perquè tinc la gran sort que m'acompanyin en aquesta última etapa.

Finalment, aquesta investigació no podria haver estat possible sense la col·laboració generosa dels participants de l'estudi, a qui estic profundament agraïda.

BIBLIOGRAPHY

[1] Obesity and overweight (n.d.) World Health Organization. https://www.who.int/news-room/fact-sheets/detail/obesity-and-overweight (accessed February 13, 2025).

[2] Lin X, Li H (2021) Obesity: Epidemiology, Pathophysiology, and Therapeutics. Frontiers in Endocrinology. https://doi.org/10.3389/fendo.2021.706978

[3] Boutari C, Mantzoros CS (2022) A 2022 update on the epidemiology of obesity and a call to action: as its twin COVID-19 pandemic appears to be receding, the obesity and dysmetabolism pandemic continues to rage on. https://doi.org/10.1016/j.metabol.2022.155217

[4] Woolcott OO, Seuring T (2023) Temporal trends in obesity defined by the relative fat mass (RFM) index among adults in the United States from 1999 to 2020: a population-based study. BMJ Open. https://doi.org/10.1136/bmjopen-2022-071295

[5] De Lorenzo A, Soldati L, Sarlo F, Calvani M, Di Lorenzo N, Di Renzo L (2016) New obesity classification criteria as a tool for bariatric surgery indication. World Journal of Gastroenterology 22(2):681-703. https://doi.org/10.3748/wjg.v22.i2.681

[6] Wu Y, Li D, Vermund SH (2024) Advantages and Limitations of the Body Mass Index (BMI) to Assess Adult Obesity. International Journal of Environmental Research and Public Health. https://doi.org/10.3390/ijerph21060757

[7] Solorzano AA, Stevens SM, Doak CM (2022) Misconceptions in the Use of Body Mass Index: A Review of the Literature. Nutrition Today 57:329–335.

[8] Budzyński J, Szukay B (2022) BMI as a Biomarker in Patients' Nutritional Assessment. Biomarkers in Nutrition, pp 597–629. https://doi.org/10.1007/978-3-031-07389-2_36

[9] Heymsfield SB, Wadden TA (2017) Mechanisms, Pathophysiology, and Management of Obesity. New England Journal of Medicine 376:254–266. https://doi.org/10.1056/nejmra1514009

[10] Jia W, Liu F (2021) Obesity: causes, consequences, treatments, and challenges. Journal of Molecular Cell Biology 13:463–465. https://doi.org/10.1093/jmcb/mjab056

[11] Stumpf MAM, Mancini MC, Correa M, Rua M (2024) Challenges in the care and treatment of patients with extreme obesity. Archives of Endocrinology and Metabolism 68:e230335. https://doi.org/10.20945/2359-4292-2023-0335

[12] Esquivel CM, Garcia M, Armando L, Ortiz G, Lascano FM, Foscarini JM (2018) Laparoscopic Sleeve Gastrectomy Resolves NAFLD: Another Formal Indication for Bariatric Surgery? Obesity Surgery 28:4022–4033. https://doi.org/10.1007/s11695-018-3466-7

[13] Lassailly G, Caiazzo R, Ntandja-Wandji LC, Gnemmi V, Baud G, Verkindt H, et al. (2020) Bariatric Surgery Provides Long-term Resolution of Nonalcoholic Steatohepatitis and Regression of Fibrosis. Gastroenterology 159:1290–1301.e5. https://doi.org/10.1053/j.gastro.2020.06.006

[14] Schmitz SMT, Kroh A, Koch A, Brozat JF, Stier C, Neumann UP, et al. (2021) Comparison of Liver Recovery After Sleeve Gastrectomy and Roux-en-Y-Gastric Bypass. Obesity Surgery 31:3218–3226. https://doi.org/10.1007/s11695-021-05390-1

[15] Łabul M, Wysocki M, Małczak P, Matyja M, Dowgiałło-Gornowicz N, Lech P, et al. (2024) The outcomes of Re-Redo bariatric surgery—results from multicenter Polish Revision Obesity Surgery Study (PROSS). Scientific Reports 14:1–9. https://doi.org/10.1038/s41598-024-52817-7

[16] Blüher M (2019) Obesity: global epidemiology and pathogenesis. Nature Reviews Endocrinology 15:288–298. https://doi.org/10.1038/s41574-019-0176-8

[17] Tacke F, Horn P, Wai-Sun Wong V, Ratziu V, Bugianesi E, Francque S, et al. (2024) EASL-EASD-EASO Clinical Practice Guidelines on the management of metabolic dysfunction-associated steatotic liver disease (MASLD). Journal of Hepatology 81:492–542. https://doi.org/10.1016/j.jhep.2024.04.031

[18] Huby T, Gautier EL (2021) Immune cell-mediated features of non-alcoholic steatohepatitis. Nature Reviews Immunology 22:429. https://doi.org/10.1038/s41577-021-00639-3

[19] Sasya M, Shalini Devi KS, Babu JK, Rayappan JBB, Krishnan UM (2020) Metabolic Syndrome—An Emerging Constellation of Risk Factors: Electrochemical Detection Strategies. Sensors 20:103. https://doi.org/10.3390/s20010103

[20] Chalasani N, Younossi Z, Lavine JE, Charlton M, Cusi K, Rinella M, et al. (2018) The diagnosis and management of nonalcoholic fatty liver disease: Practice guidance from the American Association for the Study of Liver Diseases. Hepatology 67:328–357. https://doi.org/10.1002/hep.29367.

[21] Kuchay MS, Choudhary NS, Mishra SK (2020) Pathophysiological mechanisms underlying MAFLD. Diabetes & Metabolic Syndrome: Clinical Research & Reviews 14:1875–1887. https://doi.org/10.1016/j.dsx.2020.09.026.

[22] Takahashi Y, Fukusato T (2014) Histopathology of nonalcoholic fatty liver disease/nonalcoholic steatohepatitis. World Journal of Gastroenterology 20:15539. https://doi.org/10.3748/wjg.v20.i42.15539.

[23] Neutrophils in MASLD and MASH (n.d.) https://pubmed.ncbi.nlm.nih.gov/39757200/ (accessed February 10, 2025).

[24] H&E staining of liver tissues (magnification, 200×) (n.d.) https://www.researchgate.net/figure/H-E-staining-of-liver-tissues-magnification-200-Compared-with-young-groups-hepatic_fig1_337961474 (accessed March 7, 2025).

[25] Dahm HH (2015) Immunohistochemical evaluation of a sarcomatoid hepatocellular carcinoma with osteoclastlike giant cells. Diagnostic Pathology 10:1–7. https://doi.org/10.1186/s13000-015-0274-4/figures/7.

[26] Younossi ZM, Marchesini G, Pinto-Cortez H, Petta S (2019) Epidemiology of Nonalcoholic Fatty Liver Disease and Nonalcoholic Steatohepatitis: Implications for

Liver Transplantation. Transplantation 103:22–27. https://doi.org/10.1097/tp.0000000000002484.

[27] Kleiner DE, Makhlouf HR (2016) Histology of Nonalcoholic Fatty Liver Disease and Nonalcoholic Steatohepatitis in Adults and Children. Clinics in Liver Disease 20:293–312. https://doi.org/10.1016/j.cld.2015.10.011.

[28] Harrison SA, Dubourg J (2024) Liver biopsy evaluation in MASH drug development: Think thrice, act wise. Journal of Hepatology 81:886–894. https://doi.org/10.1016/j.jhep.2024.06.008.

[29] Wang R, Lan C, Benlagha K, Camara NOS, Miller H, Kubo M, et al. (2024) The interaction of innate immune and adaptive immune system. MedComm (Beijing) 5. https://doi.org/10.1002/mco2.714.

[30] Sharma SM, Chavhan VC, Shinde SK, Shewale AB (n.d.) Immunology: The Sentinel of Health and Disease. International Journal of Pharmaceutical Research and Applications 10:426. https://doi.org/10.35629/4494-1001426441.

[31] Marshall JS, Upton JEM, Vliagoftis H, Hildebrand KJ, Byrne A, Watson W (2024) Introduction to immunology and immune disorders. Allergy, Asthma and Clinical Immunology 20:1–12. https://doi.org/10.1186/s13223-024-00932-5/tables/4.

[32] Heymann F, Tacke F (2016) Immunology in the liver—from homeostasis to disease. Nature Reviews Gastroenterology & Hepatology 13:88–110. https://doi.org/10.1038/nrgastro.2015.200.

[33] Gola A, Dorrington MG, Speranza E, Sala C, Shih RM, Radtke AJ, et al. (2020) Commensal-driven immune zonation of the liver promotes host defence. Nature 589:131–136. https://doi.org/10.1038/s41586-020-2977-2.

[34] Parlar YE, Ayar SN, Cagdas D, Balaban YH (2023) Liver immunity, autoimmunity, and inborn errors of immunity. World Journal of Hepatology 15:52–67. https://doi.org/10.4254/wjh.v15.i1.52.

[35] Cho Y, Szabo G (2021) Two Faces of Neutrophils in Liver Disease Development and Progression. Hepatology 74:503. https://doi.org/10.1002/hep.31680.

[36] Mori T, Yoshio S, Kakazu E, Kanto T (2024) Active role of the immune system in metabolic dysfunction-associated steatotic liver disease. Gastroenterology Reports (Oxford) 12:goae089. https://doi.org/10.1093/gastro/goae089.

[37] Hu Y, Schnabl B, Stärkel P (2025) Origin, Function, and Implications of Intestinal and Hepatic Macrophages in the Pathogenesis of Alcohol-Associated Liver Disease. Cells 14:207. https://doi.org/10.3390/cells14030207.

[38] Cancello R, Henegar C, Viguerie N, Taleb S, Poitou C, Rouault C, et al. (2005) Reduction of macrophage infiltration and chemoattractant gene expression changes in white adipose tissue of morbidly obese subjects after surgery-induced weight loss. Diabetes 54:2277–2286. https://doi.org/10.2337/diabetes.54.8.2277.

[39] Minervino D, Gumiero D, Nicolazzi MA, Carnicelli A, Fuorlo M, Guidone C, et al. (2015) Leukocyte Activation in Obese Patients: Effect of Bariatric Surgery. Medicine 94. https://doi.org/10.1097/MD.0000000000001382.

[40] Peiseler M, Schwabe R, Hampe J, Kubes P, Heikenwälder M, Tacke F (2022) Immune mechanisms linking metabolic injury to inflammation and fibrosis in fatty liver disease – novel insights into cellular communication circuits. Journal of Hepatology 77:1136–1160. https://doi.org/10.1016/j.jhep.2022.06.012.

[41] Grignaffini F, Barbuto F, Troiano M, Piazzo L, Simeoni P, Mangini F, et al. (2024) The Use of Artificial Intelligence in the Liver Histopathology Field: A Systematic Review. Diagnostics 14:388. https://doi.org/10.3390/diagnostics14040388.

[42] Wu B, Moeckel G (2023) Application of digital pathology and machine learning in the liver, kidney and lung diseases. Journal of Pathology Informatics 14:100184. https://doi.org/10.1016/j.jpi.2022.100184.

[43] Bankhead P, Loughrey MB, Fernández JA, Dombrowski Y, McArt DG, Dunne PD, et al. (2017) QuPath: Open source software for digital pathology image analysis. Scientific Reports 7. https://doi.org/10.1038/s41598-017-17204-5.

[44] Pixel classification — QuPath 0.5.1 documentation (n.d.) https://qupath.readthedocs.io/en/stable/docs/tutorials/pixel_classification.html (accessed March 14, 2025).

[45] Onoiu A-I, Domínguez DP, Joven J (2025) Digital Pathology Tailored for Assessment of Liver Biopsies. Biomedicines 13:846. https://doi.org/10.3390/biomedicines13040846.

[46] Chan JKC (2014) The Wonderful Colors of the Hematoxylin–Eosin Stain in Diagnostic Surgical Pathology. International Journal of Surgical Pathology 22.

[47] Exbrayat JM (2015) Microscopy: Light Microscopy and Histochemical Methods. Encyclopedia of Food and Health.

[48] Rodríguez-López S, Martínez MFE, Junquera L, García-Pola M (2021) Two-Dimensional Analysis of Digital Images through Vector Graphic Editors in Dentistry: New Calibration and Analysis Protocol Based on a Scoping Review. International Journal of Environmental Research and Public Health 18. https://doi.org/10.3390/ijerph18094497.

[49] Tigner A, Ibrahim SA, Murray I (2025) Histology, White Blood Cell. StatPearls.

[50] Donadon M, Torzilli G, Cortese N, Soldani C, Di Tommaso L, Franceschini B, et al. (2020) Macrophage morphology correlates with single-cell diversity and prognosis in colorectal liver metastasis. Journal of Experimental Medicine 217. https://doi.org/10.1084/jem.20191847.

[51] Wang M, Misakian M, He HJ, Bajcsy P, Abbasi F, Davis JM, et al. (2014) Quantifying CD4 receptor protein in two human CD4+ lymphocyte preparations for quantitative flow cytometry. Clinical Proteomics 11. https://doi.org/10.1186/1559-0275-11-43.

[52] Howden AJM, Hukelmann JL, Brenes A, Spinelli L, Sinclair LV, Lamond AI, et al. (2019) Quantitative analysis of T cell proteomes and environmental sensors during T cell differentiation. Nature Immunology 20:1542–1554. https://doi.org/10.1038/s41590-019-0495-x.

[53] Dickinson AJ, Meyer M, Pawlak EA, Gomez S, Jaspers I, Allbritton NL. (2015) Analysis of sphingosine kinase activity in single natural killer cells from peripheral blood. Integrative Biology (Cambridge) 7:392–400. https://doi.org/10.1039/c5ib00007f.

[54] Gallo G, DG, SC. (2024) Update on Obesity and Cardiovascular Risk: From Pathophysiology to Clinical Management. Nutrients 16.

[55] Jacobsen E BDMPAA. (2022) A Systematic Review of the Evidence for Non-surgical Weight Management for Adults with Severe Obesity: What is Cost Effective and What are the Implications for the Design of Health Services? Current Obesity Reports 4:356–385.

[56] O'Brien PE, Hindle A, Brennan L, Skinner S, Burton P, Smith A, et al. (2018) Long-Term Outcomes After Bariatric Surgery: a Systematic Review and Meta-analysis of Weight Loss at 10 or More Years for All Bariatric Procedures and a Single-Centre Review of 20-Year Outcomes After Adjustable Gastric Banding. Obesity Surgery 29:3–14. https://doi.org/10.1007/s11695-018-3525-0.

[57] Li Y, Yang P, Ye J, Xu Q, Wu J, Wang Y. (2024) Updated mechanisms of MASLD pathogenesis. Lipids in Health and Disease 23:117. https://doi.org/10.1186/s12944-024-02108-x.

[58] Fakhry TK, Mhaskar R, Schwitalla T, Muradova E, Gonzalvo JP, Murr MM. (2019) Bariatric surgery improves nonalcoholic fatty liver disease: a contemporary systematic review and meta-analysis. Surgery for Obesity and Related Diseases 15:502–511. https://doi.org/10.1016/j.soard.2018.12.002.

[59] Gihring A, Gärtner F, Mayer L, Roth A, Abdelrasoul H, Kornmann M, et al. (2023) Influence of bariatric surgery on the peripheral blood immune system of female patients with morbid obesity revealed by high-dimensional mass cytometry. Frontiers in Immunology 14:1131893. https://doi.org/10.3389/fimmu.2023.1131893/full.

[60] Vitiello A, Abu-Abeid A, Dayan D, Berardi G, Musella M. (2023) Long-Term Results of Laparoscopic Sleeve Gastrectomy: a Review of Studies Reporting 10+ Years Outcomes. Obesity Surgery 33:3565. https://doi.org/10.1007/s11695-023-06824-8.

[61] Meira MD, Oliveira F de SC, Coutinho LR, Leão LH de A, Vasconcelos G de P, Siqueira LT de, et al. (2023) Long-term evaluation of patients with BMI = 50kg/m2 who underwent Bariatric Surgery. Revista do Colégio Brasileiro de Cirurgiões 50:e20233397. https://doi.org/10.1590/0100-6991E-20233397-EN.

[62] Athanasiadis D, MPKSM, DS. (2021) Factors associated with weight regain post-bariatric surgery: a systematic review. Surgical Endoscopy 35:4069–4084.

[63] Waqas A, Bui MM, Glassy EF, El Naqa I, Borkowski P, Borkowski AA, et al. (2023) Revolutionizing Digital Pathology With the Power of Generative Artificial Intelligence and Foundation Models. Laboratory Investigation 103. https://doi.org/10.1016/j.labinv.2023.100255.

[64] Zhang DY, Venkat A, Khasawneh H, Sali R, Zhang V, Pei Z. (2024) Implementation of Digital Pathology and Artificial Intelligence in Routine Pathology Practice. Laboratory Investigation 104. https://doi.org/10.1016/j.labinv.2024.102111.

[65] Maretti-Mira AC, Salomon MP, Chopra S, Yuan L, Golden-Mason L. (2024) Circulating Neutrophil Profiles Undergo a Dynamic Shift during Metabolic Dysfunction-Associated Steatohepatitis (MASH) Progression. Biomedicines 12. https://doi.org/10.3390/biomedicines12051105.

[66] Shim HB, Deniset JF, Kubes P. (2022) Neutrophils in homeostasis and tissue repair. International Immunology 34:399–409. https://doi.org/10.1093/intimm/dxac029.

[67] Scapini P, Marini O, Tecchio C, Cassatella MA. (2016) Human neutrophils in the saga of cellular heterogeneity: insights and open questions. Immunological Reviews 273:48–60. https://doi.org/10.1111/imr.12448.

[68] Houshmandfar S, Saeedi-Boroujeni A, Rashno M, Khodadadi A, Mahmoudian-Sani MR. (2021) miRNA-223 as a regulator of inflammation and NLRP3 inflammasome, the main fragments in the puzzle of immunopathogenesis of different inflammatory diseases and COVID-19. Naunyn-Schmiedeberg's Archives of Pharmacology 394:2187. https://doi.org/10.1007/s00210-021-02163-6.

[69] Yan L, Wang J, Cai X, Liou YC, Shen HM, Hao J, et al. (2024) Macrophage plasticity: signaling pathways, tissue repair, and regeneration. MedComm (Beijing) 5:e658. https://doi.org/10.1002/MCO2.658.

[70] Elliott MR, Koster KM, Murphy PS. (2017) Efferocytosis Signaling in the Regulation of Macrophage Inflammatory Responses. Journal of Immunology 198:1387–94. https://doi.org/10.4049/JIMMUNOL.1601520.

[71] Li SL, Wang ZM, Xu C, Che FH, Hu XF, Cao R, et al. (2022) Liraglutide Attenuates Hepatic Ischemia-Reperfusion Injury by Modulating Macrophage Polarization. Frontiers in Immunology 13. https://doi.org/10.3389/FIMMU.2022.869050.

[72] Nawaz A, Bilal M, Fujisaka S, Kado T, Aslam MR, Ahmed S, et al. (2022) Depletion of CD206+ M2-like macrophages induces fibro-adipogenic progenitors activation and muscle regeneration. Nature Communications 13:1–12. https://doi.org/10.1038/s41467-022-34191-y.

[73] Sun D, Luo T, Dong P, et al. (2020) $CD86^{+}/CD206^{+}$ tumor-associated macrophages predict prognosis of patients with intrahepatic cholangiocarcinoma. https://doi.org/10.7717/peerj.8458

[74] Bouffette S, Botez I, De Ceuninck F. (2023) Targeting galectin-3 in inflammatory and fibrotic diseases. Trends in Pharmacological Sciences 44:519–31. https://doi.org/10.1016/J.TIPS.2023.06.001.

[75] Lu HY, Shih CM, Huang CY, Wu ATH, Cheng TM, Mi FL, et al. (2020) Galectin-3 Modulates Macrophage Activation and Contributes Smooth Muscle Cells Apoptosis in Abdominal Aortic Aneurysm Pathogenesis. International Journal of Molecular Sciences 21:8257. https://doi.org/10.3390/IJMS21218257.

[76] Cyr B, Keane RW, Vaccari JP de R. (2020) ASC, IL-18 and Galectin-3 as Biomarkers of Non-Alcoholic Steatohepatitis: A Proof of Concept Study. International Journal of Molecular Sciences 21:1–13. https://doi.org/10.3390/IJMS21228580.

[77] Barbosa P, Pinho A, Lázaro A, Paula D, Tralhão JG, Paiva A, et al. (2024) Bariatric Surgery Induces Alterations in the Immune Profile of Peripheral Blood T Cells. Biomolecules 14:219. https://doi.org/10.3390/biom14020219 .

[78] Wijngaarden LH, Taselaar AE, Nuijten F, van der Harst E, Klaassen RA, Kuijper TM, et al. (2022) T and B Cell Composition and Cytokine Producing Capacity Before and After Bariatric Surgery. Frontiers in Immunology 13:888278. https://doi.org/10.3389/FIMMU.2022.888278.

[79] Wysocki M, CK, RJ, ZP, WM, BK, JP, KW, SJ, TW, P-AM, MP, PM, MP, P-. (2023) The analysis of factors increasing the odds for type 2 diabetes mellitus remission following re-do bariatric surgery after laparoscopic sleeve gastrectomy – cohort study. *Langenbeck's Archives of Surgery* 408.

[80] Human CD & Other Cellular Antigens – ES. (n.d.).

[81] Janeway CA, Travers P, Walport M, Shlomchik MJ. (2001) Appendix II. CD Antigens. *Immunobiology: The Immune System in Health and Disease*, 5th ed. Garland Science.

[82] Hoffmann-La Roche. (2025) CONFIRM anti-CD15 (MMA) Mouse Monoclonal Primary Antibody.

[83] Hoffmann-La Roche. (2023) Galectin-3 (9C4) Mouse Monoclonal Antibody.

[84] Hoffmann-La Roche. (2023) CONFIRM anti-CD68 (KP-1) Primary Antibody.

[85] Hoffmann-La Roche. (2023) CONFIRM anti-CD4 (SP35) Rabbit Monoclonal Primary Antibody.

[86] Hoffmann-La Roche. (2023) CONFIRM anti-CD8 (SP57) Rabbit Monoclonal Primary Antibody.

[87] Hoffmann-La Roche. (2023) CD56 (MRQ-42) Rabbit Monoclonal Antibody.

[88] Hoffmann-La Roche. (2025) ultraView DAB IHC Detection Kit.

[89] Hoffmann-La Roche. (2025) OptiVIEW DAB IHC Detection Kit.

SUPPLEMENTARY MATERIAL

Table S1. *Overview of antigen expression accross different cell types, indicating which markers are associated with specific immune cell populations* [80,81].

POSITIVE CELL EXPRESSION	
Antigen	**Cell type**
CD15	Neutrophils, eosinophils, monocytes, endothelial, natural killer
CD68	Monocytes, macrophages, neutrophils, basophils, large lymphocytes, dendritic
CD4	CD4 lymphocytes, endothelial
CD8	CD8 lymphocytes, endothelial
CD56	Natural killer, Natural killer T
Galectin-3	Inflammation (secreted by various immune cells)

R PACKAGES AND LIBRARIES

```
install.packages('ggplot2')
library (ggplot2)
library (tidyverse)
library (ggpubr)
library (readxl)
library (MASS)
library (car)
library (dplyr)
library (writexl)
library (tidyr)
options (scipen = 999)
```

Code box S1. *Script used to install and import the packages and libraries required for conducting the statistical analysis.*

POSITIVE CELL COUNT AND DENSITY

```
# Load data
# List files in directory
temp = list.files (path = "C:/Users/ponts/Desktop/CD15_results_Adriana",
pattern = "*.txt",
full.names = TRUE )

# Apply read_delim to all of them
lista <- lapply (
temp,
readr : : read_delim,
delim = "\t",
escape_double = FALSE,
trim_ws = TRUE
)

# Rbind the generated list to create a dataframe
super_CD15 <- data.table : : rbindlist (lista, fill = TRUE)
table (super_CD15 $ Classification)

# Filter the dataset so that all the positive cells have an area grater
than 110um2
super_CD15 <- super_CD15 %>%
filter ( ! (Classification == "Positive" & `Cell: Area` < 110))

#Filter the dataset to avoid false negatives. Hematoxylin stain is at
least 0,05.
super_CD15 <- super_CD15 %>%
filter (! (Classification == "Negative" &
              `Cell: Hematoxylin OD mean` < 0.05))

test_CD15_fin <- super_CD15 %>%
        group_by (Image) %>%
        summarise (
                Positive_Count = sum(Classification == "Positive", na.rm = TRUE),
                Negative_Count = sum(Classification == "Negative", na.rm = TRUE)
        ) %>%
        mutate (Prop_Count_Neutrophils = Positive_Count / (Negative_Count +
        Positive_Count))

# Add the column tissue_area_um2 to the dataset
tissue_area <- super_CD15 %>%
        group_by (Image) %>%
        summarise  (tissue_area_um2 = sum  (`Cell: Area`, na.rm = TRUE))
```

```
# Add the data based in the column "Image"
test_CD15_fin <- test_CD15_fin %>%
        left_join (tissue_area, by = "Image")

#Transform um2 to mm2
test_CD15_fin$tissue_area_mm2 <- test_CD15_fin$tissue_area_um2/1000000
test_CD15_fin$CD15_density <- test_CD15_fin$Positive_Count /test_CD15_fin
$tissue_area_mm2

# Verify structure after extraction
str (test_CD15_fin)
write_xlsx (test_CD15_fin, path =
"C:/Users/ponts/Desktop/CD15_results_Adriana/CD15_analysis/test_CD15_ul
timo.xlsx")
```

Code box S2. *Script used for the preprocessing and quantification of CD15-positive cells. It filters out potential false positives and false negatives, aggregates counts by image and calculates the proportion and density of positive cells relative to the tissue area. This approach ensures accurate estimation of positive cells density per mm² for subsequent statistical analyses. The same type of script was applied for all antibodies.*

BOX-PLOTS FOR THE CHARACTERIZATION OF IMMUNE CELL PROFILES BEFORE AND AFTER SURGERY-INDUCED WEIGHT LOSS

```
# Load the dataset
CD15_final <- read_xlsx (

      "C:/Users/ponts/Desktop/CD15_results_Adriana/CD15_analysis/test_C
      D15_ultimo.xlsx"
)

# Perform a Wilcoxon test to determine statistical differences
wilcox.test (Prop_Count_Neutrophils ~ Intervention, data = CD15_final)

# Boxplot with p-value of CD15+ cells proportion
boxplot_cd15_prop_count <- ggplot (CD15_final, aes(x = as.factor (Intervention), y
Prop_Count_Neutrophils)) +
geom_boxplot (aes(fill = as.factor (Intervention)), width = 0.2) +
stat_compare_means (method = "wilcox.test", label = "p.signif") +
labs (title = "Comparación de Prop_Count_Neutrophils por Intervención", x =
"Intervention", y = "Prop Count Neutrophils") +
theme_minimal () +
scale_fill_manual (values = c ("#00AFBB" , "#E7B800"))
```

```
ggsave (
"C:/Users/ponts/Desktop/CD15_results_Adriana/CD15_figures/prop_CD15.pdf
",
plot = boxplot_cd15_prop_count,
width = 15,
height = 15
)

summary  (CD15_final $ Prop_Count_Neutrophils[CD15_final$Intervention == 1])
summary (CD15_final$Prop_Count_Neutrophils[CD15_final$Intervention == 2])

# Boxplot with p-value of CD15+ cells density
boxplot_cd15_density <- ggplot  (CD15_final, aes(x = as.factor (Intervention), y =
CD15_density)) +
geom_boxplot (aes(fill = as.factor (Intervention)), width = 0.2) +
stat_compare_means(method = "wilcox.test", label = "p.signif") +
labs (title = "Comparación de CD15+cells/mm2 por Intervención", x =
"Intervention", y= "CD15+cells/mm2”) +
theme_minimal  () +
scale_fill_manual  (values = c("#00AFBB", "#E7B800"))

ggsave(
"C:/Users/ponts/Desktop/CD15_results_Adriana/CD15_figures/density_CD15.
pdf",
plot = boxplot_cd15_density,
width =  15,
height =  15
)

summary  (CD15_final$ CD15_density[CD15_final$ Intervention == 1])
summary (CD15_final$ CD15_density[CD15_final$ Intervention == 2 ])
wilcox.test (CD15_density ~ Intervention, data =  CD15_final)
```

Code box S3. *Script for statistical comparison and visualization of CD15-positive cells proportion and density across intervention groups. A Wilcoxon rank-sum test was used to assess differences in cell proportions and cell density per mm². The same type of script was applied for all antibodies.*

MULTIPLE BOXPLOTS FOR THE RELATIONSHIP BETWEEN IMMUNE CELL INFILTRATION CHANGES AND LIVER DAMAGE PARAMETERS

```
# Load the dataset
dataset_correl <-
read_xlsx("/Users/adrianacalvorecasens/Desktop/UNI/4rt/TFG/CORRELACIONS_ADRIAN
A_TFG/CORRELACIONS_CD15/Copia de Dataset_STEP2_URV.xlsx",
                  sheet = "dataset_correlations_CD15")

# Make sure the variable is cathegoric
dataset_correl$Steatosis_score_Diff <- as.factor(dataset_correl$Steatosis_score_Diff)

# Create the plot with multiple comparations (Kruskal-Wallis + Wilcoxon)
multiple_boxplot_steatosis_score <- ggboxplot(dataset_correl,
       x = "Steatosis_score_Diff",
       y = "CD15_count_diff",
       color = "Steatosis_score_Diff",
       palette = "jco",
       add = "jitter") +
 stat_compare_means(method = "kruskal.test", label.y =
max(dataset_correl$CD15_count_diff, na.rm = TRUE) * 1.1) +
 stat_compare_means(method = "wilcox.test",
              comparisons = combn(levels(dataset_correl$Steatosis_score_Diff), 2, simplify =
FALSE),
              label = "p.signif")

# Save the plot in PDF format
ggsave(
 filename =
"/Users/adrianacalvorecasens/Desktop/UNI/4rt/TFG/CORRELACIONS_ADRIANA_TFG/CO
RRELACIONS_CD15/CD15_count_steatosis.pdf",
 plot = multiple_boxplot_steatosis_score,
 device = "pdf",
 width = 10,
 height = 6,
 units = "in"
)
```

Code box S5. Script for the performing of statistical analysis and generation of visualizations. *For each analysis, the variable of interest was converted to a categorical variable using the as.factor() function. Boxplots were constructed with the ggboxplot() function, where the x-axis represented the categorical variable (a liver damage parameter) and the y-axis represented the continuous variable (positive cells count or density). Statistical comparisons were made using the Kruskal-Wallis test to assess global differences between groups, followed by pairwise comparisons using the Wilcoxon*

test for each pair of levels within the categorical variable. The results of these statistical tests were directly added to the plot using the stat_compare_means() function. The plots were then saved in PDF format, with dimensions customized to suit the analysis. The same type of script was applied for all antibodies.

BOXPLOTS FOR THE RELATIONSHIP BETWEEN SIGNIFICANT IMMUNE CELL POPULATIONS AND OBESITY-RELATED COMORBIDITIES

```
# Read the dataset
df <- read_excel("/Users/adrianacalvorecasens/Library/CloudStorage/OneDrive-URV/dataset_boxplots_correlations_objective3.xlsx",
           sheet = "T2DM")

# Correct the punctuation
df$Count_CD15 <- as.numeric(gsub(",", ".", df$Count_CD15))

# Label the variable
df$T2DM <- factor(df$T2DM, levels = c(0, 1), labels = c("No", "Sí"))

# Create the boxplot with Wilcoxon test
p <- ggboxplot(df,
          x = "T2DM",
          y = "Count_CD15",
          color = "T2DM",
          palette = c("#66c2a5", "#fc8d62"),
          add = "jitter",
          title = "CD15 vd T2DM",
          xlab = "T2DM",
          ylab = "CD15-positive cells proportion") +
   stat_compare_means(method = "wilcox.test", label = "p.format")

# Save the plot in PDF format
ggsave(filename =
"/Users/adrianacalvorecasens/Desktop/UNI/4rt/TFG/CORRELACIONS_ADRIANA_TFG/boxplots objectiu 3/CD15_vs_T2DM.pdf",
     plot = p,
     width = 7,
     height = 5)
```

Code box S4. *Script for assessing the distribution of CD15- positive celsl proportion according to the presence of T2DM. The dataset was imported and decimal punctuation was corrected. The T2DM variable was converted to a categorical factor with labeled levels. A boxplot was generated using the ggboxplot() function, where the x-axis represented T2DM status and the y-axis corresponded to CD15-positive cells proportion. Statistical comparison between the two groups was performed using the Wilcoxon rank-sum test. The p-value was added to the plot using the stat_compare_means() function. Visualizations were*

exported in PDF format with customized dimensions. This approach was applied consistently across analyses involving different antibodies.

DETAILED PROTOCOL FOR IHC STAINING

Both the *ultra*View Universal DAB Detection Kit and the OptiView DAB IHC Detection Kit detect specific mouse and rabbit primary antibodies bound to an antigen in formalin-fixed, paraffin-embedded tissue sections, or in frozen tissue sections. One of the two kits is selected for each antibody according to the specifications detailed in its corresponding protocol (*Table S2*).

Table S2. *Primary antibodies and their corresponding detection kits used for IHC staining [82–87].*

Antibody	Detection kit
Anti-CD15	OptiView DAB IHC Detection
Anti-CD68	OptiView DAB IHC Detection
Anti-CD4	*ultra*View Universal DAB Detection
Anti-CD8	*ultra*View Universal DAB Detection
Anti-CD56	*ultra*View Universal DAB Detection
Anti-Gal3	*ultra*View Universal DAB Detection

In the ultraView kit, the specific antibody is detected by a cocktail of enzyme-labeled secondary antibodies, while in the OptiView kit, it is detected by a specific secondary antibody that is bound by an enzyme-labeled tertiary antibody. The complex is then visualized with hydrogen peroxide substrate and DAB chromogen, which produces a brown precipitate that is readily observed under light microscopy.

The staining protocol (*Table S3*) consists of numerous steps in which reagents are incubated the prefetermined times at specific temperatures, depending on the antibody (*Table S4*). At the end of each incubation step, the Benchmark IHC instrument washes the sections to remove unbound material and applies a liquid coverslip which minimizes the evaporation of the aqueous reagents from the slide.

Table S3. *Procedure for IHQ staining using OptiView and ultraViewDAB IHC Detection kits [88,89].*

Step	Detail
1	Apply slide bar code label which corresponds to the protocol to be performed.
2	Load the primary antibody, appropriate detection kit dispensers, and required accessory reagent onto the reagent tray and place them on the instrument.
3	Check bulk fluids and empty waste.
4	Load the slides onto the instrument.
5	Start the staining run.
6	At the completion of the run, remove the slides from the instrument.

Table S4. *Predetermined IHC staining incubation steps and times for each antibody [82–87].*

Antibody	Deparaffination	Cell conditioning	Antibody (primary)	Counterstain	Post counterstain
Anti-CD15	Selected	64 minutes 100ºC	16 minutes 36ºC	Hematoxylin II, 4 minutes	Bluing, 4 minutes
Anti-CD68	Selected	Standard	20 minutes 36ºC	Hematoxylin II, 4 minutes	Bluing, 4 minutes
Anti-CD4	Selected	Standard	32 minutes 36ºC	Hematoxylin II, 4 minutes	Bluing, 4 minutes
Anti-CD8	Selected	64 minutes 95ºC	20 minutes 36ºC	Hematoxylin II, 4 minutes	Bluing, 4 minutes
Anti-CD56	Selected	Standard	16 minutes 36ºC	Hematoxylin II, 8 minutes	Bluing, 4 minutes
Anti-Gal3	Selected	Standard	16 minutes 36ºC	Hematoxylin II, 8 minutes	Bluing, 4 minutes